INDIRECT ADDITIVE MANUFACTURING OF CERAMICS

A Thesis

by

DIPTANSHU

Submitted to the Office of Graduate and Professional Studies of
Texas A&M University
in partial fulfillment of the requirements for the degree of

MASTER OF SCIENCE

Chair of Committee,	Chao Ma
Co-Chair of Committee,	Bruce Tai
Committee Member,	Hong Liang
Head of Department,	Andreas A. Polycarpou

August 2018

Major Subject: Mechanical Engineering

ABSTRACT

Additive manufacturing of ceramics has gained a lot of impetus recently due to its ability to do away with the costs of machining ceramics. In this study, the feasibility of two popular methods: indirect selective laser sintering (SLS) and vat photopolymerization was studied. The focus of this research is on feedstock material preparation of these two processes.

Firstly, temperature induced phase separation (TIPS) was used to prepare three different powders containing varied amounts of polyamide and alumina composite microspheres. Flowability versus sinterability of the feedstock composite powder was studied. The results showed that as the fraction of polyamide in the composite powder increased, the flowability of the powder increased, however the sinterability decreased. Inferentially, a fine balance of flowability versus sinterability must be maintained in order to produce dense crack free alumina 3D parts by indirect SLS.

Secondly, vat photopolymerization was chosen to produce 3D alumina parts using the commercial vat photopolymerization printer (Nobel Superfine, XYZprinting). Four green bodies using a photopolymerizable ceramic suspension were created. All were subjected to the same parameters of thermal processing. A quantitative study of the amount of open and closed pores and their dependence on the size of the sintered parts was done. The lowest porosity was observed in the smallest cubes (5 mm).

Finally, green bodies using the vat photopolymerization technique were created using three monomodal and three bimodal ceramic suspensions consisting of varying volumes of alumina particles in an in-house photopolymerizable resin. A quantitative study of the

apparent solid and bulk densities of the specimens was done. The sample containing 0.3 µm particles achieved the highest density among the monomodal suspensions. The sample containing 0.3 µm & 0.8 µm particles achieved the highest density among the bimodal suspensions. This work demonstrated that adding a small amount of a finer ceramic powder as dopant to a larger sized ceramic powder significantly improved the sinterability of the green part.

The promising nature of vat photopolymerization of ceramics presents great opportunities for the production of high density ceramics using a bottom-up 3D printer by optimizing the fractions of different components of a photopolymerizable ceramic suspension.

ACKNOWLEDGEMENTS

I would like to extend my gratitude and a heartfelt thank you to my research advisor Dr. Chao Ma for his excellent guidance, support and encouragement throughout the duration of this research work and for being a wonderful advisor. I would also like to thank my research committee co-chair Dr. Bruce Tai and research committee member Dr. Hong Liang, for their continued guidance and support.

I would also like to thank XYZprinting for providing us with the Nobel Superfine printer which I used for my experiments. I would like to thank my lab mates Wenchao Du, Ming Li, Guanxiong Miao and Xiaorui Ren for their help during my research. A great thanks to my dear friends at Texas A&M for their continued support and for making this journey a joyous experience.

I would like to extend my gratitude to the department head Dr. Andreas A. Polycarpou and other faculty members of the Department of Mechanical Engineering who helped me immensely from time to time.

A great thank you to the faculty members and the administrative coordinator Mrs. Robin Watkins at the Department of Engineering Technology and Industrial Distribution and Texas A&M University. I would also like to thank the Libraries for the resources used during this research.

CONTRIBUTORS AND FUNDING SOURCES

All work for the thesis was completed by the student, under the advisement of Dr. Chao Ma of the Department of Engineering Technology and Industrial Distribution and the Department of Mechanical Engineering. I would like to acknowledge Dr. Bruce Tai and Dr. Hong Liang for their guidance and support during the research work.

There are no outside funding contributions to acknowledge related to the research and compilation of this document.

TABLE OF CONTENTS

LIST OF FIGURES

Page

CHAPTER I

INTRODUCTION

1.1 MOTIVATION

Ceramics find their application in a myriad of applications ranging from the biomedical to the military industries. The high hardness, chemical stability and wear resistance are some properties that are popularly leveraged. The high hardness of the ceramics makes its tooling difficult resulting in it accounting for 70-80% of the total production cost of ceramics. The main motivation of the research study is to identify a promising technique for the additive manufacturing (AM) of ceramics out of the seven ASTM defined AM methods and develop materials and methods for the same.

"AM is the process of joining materials to make objects from 3D model data, usually layer upon layer, as opposed to subtractive manufacturing methodologies" [ASTM 2012]. One of the principal advantages of AM is that it can be used to build intricate shapes with a wide variety of materials including ceramics, metals, polymers, composites, etc. AM of ceramics gained impetus in the early 1990s but was mainly used to create prototypes. However, in recent years due to advances in the technology of the AM machines and development of new materials it is possible to produce highly dense ceramics structures. AM does away with the need for machining which in case of ceramics can account for up to 70-80% of the overall component cost [Klocke 1997]. AM is considered a transformative ceramic manufacturing technique to create intricate or personalized parts [Utela 2008, Decker 2014, Yeong 2013, Zocca 2015, Gmeiner 2015, Bertsch 2003, Trombetta 2017, Du 2017]. AM is broadly categorized into seven classifications for easy grouping of the present and even future technologies [ASTM 2012]. All of the seven process categories have been attempted

for the manufacturing of ceramic parts [Utela 2008, Decker 2014, Yeong 2013, Zocca 2015, Gmeiner 2015, Bertsch 2003, Trombetta 2017, Du 2017].

1.2 RESEARCH OBJECTIVES

I. Investigate the feasibility of Temperature Induced Phase Separation (TIPS) method to produce alumina feedstock for Indirect Selective Laser Sintering (SLS).

II. Selection of components for an alumina suspension for a bottom-up Digital Light Processing (DLP) XYZprinting Superfine Nobel printer.

III. Investigate the feasibility of vat photopolymerization to produce alumina 3D objects.

CHAPTER II

LITERATURE REVIEW

2.1 CERAMIC AM TECHNOLOGIES

AM processes are categorized into seven divisions by ASTM (Table 1).

Classified by ASTM/ISO						
Single Step		Multi Step				
Directed Energy Deposition	Powder Bed Fusion	Vat Polymerization	Material Jetting	Material Extrusion	Sheet Lamination	Binder Jetting

Table 1: Classification of AM processes to produce ceramics

These processes can be further categorized in two categories of AM processes which as defined by the ISO/ASTM standard are: (i) the single step processes (also called 'direct' processes), in which 3D structures are formed in a single operation in which the geometrical shape and material properties of the intended product are achieved simultaneously and (ii) the multi-step processes (also called 'indirect' processes), in which the parts are fabricated in two or more operations where the first step typically provides the geometrical shape and the following step provides the part with the intended material properties [Deckers 2014]. The indirect processes usually use a sacrificial binder which provides a green matrix to the ceramic particles suspended in it. After the thermal post processing which includes de-binding and sintering processes, the binder is decomposed and the ceramic particles get compacted together to form the final ceramic body. The only single step processes are known to be directed energy deposition and the (single step) powder

bed fusion techniques essentially Selective Laser Melting (SLM) and direct Selective Laser Sintering (SLS).

2.1.1 DIRECTED ENERGY DEPOSITION

The Direct energy deposition (DED) methods, defined as "additive manufacturing processes in which focused thermal energy is used to fuse materials by melting as they are being deposited". It is a 3D printing method which is commonly used to repair or augment additional material to existing components [Edgar 2015]. A typical DED machine consists of a nozzle mounted onto a multi-axes arm, which transfers molten material onto the specified surface, where it solidifies. This process is similar in principle to the material extrusion process, but the nozzle can move in multiple directions and is not fixed to a specific axis. The material, which can be deposited from a number of angles due to the multiple axes machine, is molten upon deposition with a heat source which could be a laser arc, or electron beam. The process can be used with a variety of materials including polymers and ceramics, but is typically used with metals, the feedstock for which can be in the form of either powder or wire. Though DED can help produce parts with high surface finish, but it suffers from mainly two problems: materials wastage and cracking of ceramic parts due to strong thermal gradients during their forming.

2.1.2 POWDER BED FUSION

Powder bed fusion processes are defined as "additive manufacturing process in which thermal energy selectively fuses regions of a powder bed" [ASTM 2012]. In this technology, a 3D structure is formed by the deposition of successive layers of powder and subsequent sintering/melting. In the literature, three different powder layer deposition systems can be identified: conventional deposition, slurry-based deposition and aerosol-assisted spray deposition. The advantage of this

process is that it can help achieve high dimensional accuracy but the parts produced using this process suffer from thermal cracks.

a) CONVENTIONAL DEPOSITION SYSTEM

In this deposition technique, large powder particles can be deposited (> 5 μm) on the powder bed. The flow of the powder is governed by the gravity forces. The main problem of cracks on the 'printed' parts can be overcome by decreasing the thermal gradients in the parts. This can be achieved by pre-heating the system at a high temperature [Nachum 2016].

b) SLURRY COATING

A SLM device with a slurry coater was developed at the National Taipei University of Technology, [Tang 2013]. Clay was used as an inorganic binder for the silica powder during the drying process. During laser scanning, dried silica-clay layer was fully melted.

c) AEROSOL SPRAY DEPOSITION

Wu et al [Wu 2007] used aerosol-assisted spray deposition of a ceramic suspension to prepare powder beds for subsequent layer scanning. The alumina suspension was prepared by adding 5 wt. % alumina powder to an ethanol solvent with 0.2 wt. % of polyacrylic acid (PAA) dispersant. During the laser irradiation of the alumina powder beds, the PAA evaporated and the submicron alumina particles were melted to form a liquid phase, which facilitated densification by means of liquid-phase sintering.

2.1.3 VAT PHOTOPOLYMERIZATION

Vat photopolymerization processes are defined as "additive manufacturing processes in which liquid photopolymer in a vat is selectively cured by light-activated polymerization" [ASTM 2012]. During the vat photopolymerization process ceramic powder are suspended in a monomer(s)/oligomer(s) doped with a photoinitiator. This suspension is then irradiated by a UV

light. The energy of the UV radiation causes the monomer(s)/oligomer(s) to polymerize and harden. This hardened polymer forms the green body matrix containing the ceramic particles. After de-binding the resulting polymer and sintering the structural material in a furnace, the final ceramic part is obtained. The main advantage of this process lies in the fact that it can produce parts with high dimensional accuracy and low surface roughness. One of the disadvantages associated with this process is the fact that it consumes a large amount of the sacrificial binder.

2.1.4 MATERIAL JETTING

The Material jetting methods, defined as "additive manufacturing processes in which droplets of build material are selectively deposited" [ASTM 2012]. The two commonly used methods in material jetting are:

I. Inkjet Printing [Williams 2008, Sirringhaus 2003, Ebert 2009, Özkol 2010, Hon 2008]. During inkjet printing (IJP), a suspension containing ceramic powder particles is deposited from a print nozzle. The print nozzle selectively deposits single droplets of the suspension onto a substrate. Upon contact, the droplets undergo change of phase, creating a solid part.

II. Aerosol jet printing [Sukeshini 2013, Grida 2003]. In this method, a focused suspension of droplets containing fine ceramic particles in a gas are used as the printing media.

The principal advantages of this process are that it produces parts with low surface roughness and it is capable of producing parts using multiple different materials. The drawback of the process is that it uses large amounts of sacrificial binder.

2.1.5 MATERIAL EXTRUSION

The Material extrusion methods, defined as “additive manufacturing process in which material is selectively dispensed through a nozzle or orifice” [ASTM 2012]. The most common method in material extrusion is the fused deposition of ceramics (FDC) [Grida 2003, Yardimci 1996, Venkataraman 2000]. In FDC, a thermoplastic filament has ceramic particles dispersed in it. Layer by layer, the flexible filament is partially melted and extruded from a moving deposition head onto a static workstation.

The popularity of the Materials Extrusion processes like the FDC owe to the fact that it is a cost effective technique and can use multiple materials to build a part. The main limitation of the process is that it the surface finish of the parts produced is poor.

2.1.6 SHEET LAMINATION

Sheet lamination is defined as “additive manufacturing process in which sheets of material are bonded to form an object” [ASTM 2012]. Laminated Object modelling (LOM) is the most common process in this category. The LOM process consists of a system that deposits subsequent layers of green ceramic tape-cast. These layers are unwound onto the working bed where a CO_2 laser shapes the outline of each layer according to the CAD model of the part. A heated roller mechanism is used to thermally activate the tape’s binder system and to laminate the sheet to the previous layer. The ceramic tape-cast layers may contain more than 40 wt. % ceramic powder in them. The green part after being formed is de-bound and sintered to form the final ceramic structure. One of the principal advantages of this process is that it produces very good surface finish as it uses green ceramic tapes. The main disadvantage of this process is that delamination main occur during the de-binding process which may increase the cracks on the surface causing increased porosity.

2.1.7 BINDER JETTING

Binder jetting, sometimes called (indirect) 3D printing, is defined by ASTM as "additive manufacturing processes in which a liquid bonding agent is selectively deposited to join powder materials" [ASTM 2012]. In the first part of this process, the powder roller spreads out a thin layer of powder which is fed from the powder feedstock onto the build platform, which thereby forms the powder bed. Then the print head jets binder onto the areas that have been pre-defined by the layer profile of the CAD model data and then the powder particles in the selected areas are bound with neighboring particles due to the binder. After the first layer is completed, the build platform is lowered by a predefined layer thickness and a new powder layer is spread onto that finished layer. These steps are repeated until the part is completed. Having printed the green part, de-binding and sintering are applied to obtain the final ceramic part. The main advantages of binder jetting are that it consumes minimal sacrificial binder and overhung parts do not need any support structures. The main disadvantage of this process is that it produces parts with high porosity and low resolution.

2.2 INDIRECT POWDER BED FUSION OF CERAMICS

The indirect powder bed fusion (PBF) technique uses a composite powder as the starting material. This composite powder consists of sacrificial binder along with the ceramic particles. When a laser beam is irradiated on a powder bed containing the composite powders the organic sacrificial binder melts and causes the ceramic particles to fuse together [Deckers 2014]. This forms the green body which needs thermal processing to form the final brown or sintered part. This thermal post processing consists of the de-binding and the sintering process. During the de-binding process the organic binder is decomposed and during the sintering phase the material diffusion takes place which helps in further densification of the desired ceramic 3D structure.

2.2.1 ADVANTAGES OF INDIRECT POWDER BED FUSION

The 3D ceramic structures formed using the PBF technique usually shows poor density and hence poor mechanical properties. On the other hand, the indirect PBF approach is known to create crack free ceramic structures. However, the complete densification of the parts is hindered by the fact that there remain some voids between the composite powder particles. These voids are not removed during the de-binding and the sintering phase [Deckers 2014].

2.2.2 MATERIALS USED IN INDIRECT POWDER BED FUSION

An eclectic range of ceramic powders and binder materials, both organic and inorganic have been known to be used using the indirect PBF process. Various ceramic materials like Al_2O_3, Al_2O_3-B_2O_3. Al_2O_3-glass-B_2O_3, AL_2O_3-ZrO_2-TiC, apatite-mullite, graphite, K_2O-Al_2O_3-SiO_2, SiO_2, SiC, ZrO_2 and ZrB_2 [Deckers 2014] have been used with the indirect PBF method. Different binder materials like long-chain fatty acids, waxes, thermosets and thermoplastics. Also, a combination of some of these binder materials maybe used.

2.2.3 TECHNOLOGIES FOR INDIRECT POWDER BED FUSION

a) CONVENTIONAL DEPOSITION TECHNIQUES

These employ the use of a roller or a doctor blade to spread a layer of the composite powder on the powder bed each time before the laser processing is done. Once each layer is processes by the scanning laser the powder bed is lowered by the distance of a layer's thickness and the second layer is spread on the powder bed by the deposition mechanism (roller or a doctor blade). This process continues till the final green body is produced.

b) SLURRY COATING

This technology was developed at the National Taipei University of Technology in Taiwan. Silica powder was used in combination with clay. The silica powder acted as the ceramic structural

material and the clay acted as the inorganic binder. An aqueous slurry of the aforementioned components was formed, deposited and dried. The laser scanning melted the clay particles which acted as the bonding between the silica particles. These green bodies were then de-bound and sintered to form the final brown silica parts.

2.3 VAT PHOTOPOLYMERIZATION OF CERAMICS

2.3.1 ADVANTAGES OF VAT PHOTOPOLYMERIZATION

In order to produce dense ceramic parts, three basic criteria have to be met. These are [Nachum 2016]:

I. The particle and the pore distribution should be homogeneous and the porosity must be minimal.
II. During the thermal processing process, the temperature and pressure gradients which cause cracks to form and propagate should be avoided.
III. Surface roughness of each layer should be minimal.

The first requirement strongly favors the use of suspensions or pastes in the AM processes to avoid the use of dry powders. The use of powders introduces the major problem of flowability versus sinterability. Van der Waals forces between dry powder particles lead to particle sticking and inhomogeneous particle arrangement in a powder bed printer when particle diameters are below 20 μm. The use of granules in powder bed processes to overcome the problem of bad flowability is not very encouraging as sufficient pressure is not applied on the powder bed during the process, therefore the granules essentially remain spherical. During the sintering process of the granules, the intergranular pores prevent the full densification of the compacts. If coarse ceramic powders

are used as raw material, their flowability is fine, but the large pores between the coarse particles inhibit complete densification as well.

The second requirement means that the forming process be separated from the heat treatment process. In direct processes such as direct energy deposition and powder bed fusion which use local heating, the time for material transfer by diffusion which is the main requirement to form dense ceramic structures is usually not enough. Moreover, strong temperature gradients occur which cause crack in the 3D structures. Though measures like the preheating of powder bed structures and doping the feedstock with specific nanoparticles to shorten the densification time using the melt phases have been investigated, these introduce a lot of undesired restrictions.

The third requirement often constraints the use of pastes as starting feedstock. High viscosity during the forming process in the Material Extrusion processes leads to low surface quality especially in parts with circular features and therefore leads to deterioration of the mechanical properties [Agarwala 1996]. Hence the motivation to use a suspension as the feedstock material is very strong. Inkjet printing, Aerosol-assisted spray deposition and vat photopolymerization are the three major techniques which use suspension as the starting material. Inkjet printing and aerosol-assisted spray deposition suffer from poor dimensional control especially in the direction perpendicular to the substrate, whereas the vat polymerization process exhibits exceptional dimensional control and surface finish.

Vat photopolymerization is a technique that follows all the criteria and does away with the flowability problems faced in other ceramic AM techniques such as the powder bed processes. Vat photo polymerization can be used to manufacture high-resolution custom ceramic parts. Vat photo polymerization is also capable of producing porous as well as fully dense parts.

2.3.2 VAT PHOTOPOLYMERIZATION PROCESS PHYSICS

Vat photopolymerization systems form 3D objects by selectively curing photocurable resins either by laser beam scanning or by UV radiation one layer at a time. This process has been investigated widely with regards to the production of ceramic green bodies. Low viscosity ($\leq$ 3 Pa·s) at 25 s^{-1} [Jang 2000] is an essential factor for an effective recoating and a low recoating time. It is also important that the cure depth of the ceramic loaded suspension be at least equal to the layer thickness. The optical transparency of the suspension is a key factor which determines the penetration depth of the light radiation. The presence of the ceramic particles in the suspension scatters the light. This scattering of the light causes a certain growth in the final dimension of the green bodies printed out. The intensity of the light falling on the layer to be cured depends on a number of factors, including particle size, refractive index of the ceramic particles, the physical properties of the resin, etc. During the formation of each layer according to the CAD model, photoinitiaters in the suspension are activated which release free radicals. These free radicals initiate the polymerization of the monomers and it increases until the gelling starts and the resin becomes a soft solid [Halloran 2016]. The cure depth (Cd) as a function of the exposure energy per unit area (E) is given by [Halloran 2011]

$$C_d = D_p \ln(\frac{E}{E_c})$$

where Dp is a sensitivity parameter called depth of penetration, and Ec is the critical exposure energy per unit area. Both parameters are determined by the composition of the resin, and the material, size, and fraction of the ceramic particles [Halloran 2011]. Photopolymerization is found to perform well with ceramics of low refractive index such as silica (SiO_2) and alumina (Al_2O_3) [Singh 2011, Bogue 2016].

2.3.3 FEEDSTOCK MATERIALS FOR VAT PHOTOPOLYMERIZATION

The two basic components of a photopolymerizable resin are base monomer(s) and photo-initiator(s). The ceramic suspension consists of a ceramic powder in addition to the monomer and a photoinitiator. Diluents and dispersants may be added to reduce the viscosity of the final resin as viscosity is a critical factor in vat photopolymerization techniques [Griffith 1996]. The final ceramic suspension may contain as many as 5 components which can include the base monomer(s), photoinitiator, diluent, dispersant and the ceramic powder particles. A stable suspension of ceramic powder dispersed in liquid monomer at a high solid loading with viscosity ≤ 3 Pa·s at 25 s^{-1} is highly desirable in stereolithography. The suspension should typically contain a high volume of ceramic particles, (50–60 vol. %) to achieve a high green density and minimize the shrinkage and the porosity of the sintered part upon the decomposition of the organic phase contained in the green body, while being fluid enough for use in a stereolithography machine.

a) MONOMER(s)/OLIGOMER(s)

The monomer(s)/oligomer(s) form the matrix of the green composite. The monomers and oligomer form the base of the resin that polymerizes and crosslinks during the manufacturing process. The most common monomers are acrylate-based. Other resin bases besides acrylate are epoxy [Gu 2017], vinylpyrrolidone (VP) [Gallardo 2017], polypropylene fumarate (PPF) [Abdelrasoul 2017], and polyvinylsilazane [Pham 2006]. In some of the epoxy-based resin, there was also acrylate-based resin incorporated into the mixture. In the experiment performed by do Santos et al., multiacrylate monomers (45–50%) and epoxies (15–25%) were used [Dos Santos 2011]. The type of resin that should be chosen depends on the application and refractive index. Wozniak et al. used an acrylate-based resin with silica since they have similar refractive indexes. The purpose of

having a similar refractive index is to limit the Van der Waals attraction [Wozniak 2011]. Transparency of the slurry can also be improved by matching the refractive indexes.

b) DILUENTS

Diluents are used to help change the viscosity of the resin. The viscosity of the resin with reinforcement material needs to be under 3 Pa·s at 25 s^{-1}. This is especially important with the incorporation of nanoparticles in a resin, because they have a large effect on increasing the viscosity.

c) PHOTOINITIATOR

The basic principle behind the Vat photopolymerization is that curing of the resins occur due to the radical formation and propagation by the photoinitiator under the influence of the energy from the UV radiation. It is very important that the photoinitiator which absorbs strongly in the range of the wavelength of the incident radiation is chosen.

d) DISPERSANTS

As discussed before the viscosity of the ceramic suspension should be ($\leq$ 3 Pa·s) at typically at 25 s^{-1} to act as a stable suspension. If the viscosity of the suspension increases more than the 3 Pa·s at low shear rates it becomes difficult for the suspension to form homogeneous layers in the case of machines using the bottom up approach. Dispersants are mainly used to make a suspension stable by minimizing the attractive forces between the ceramic particles and introducing repulsive forces. Both long chain and short chain molecules of dispersants have been known to act stabilize the suspension providing low sedimentation rates of the ceramic particles.

e) CERAMIC PARTCILES

Various ceramic particles have been investigated for the use of vat photopolymerization. Some of these popularly include Alumina, Zirconia, Silica, Barium Titanate etc [Deckers 2014]. Some

important considerations regarding the ceramic particles may include properties like the size and shape of the particles, refractive index and the ceramic volume fraction suspended in the resin.

2.3.4 CERAMIC VAT PHOTOPOLYMERIZATION TECHNOLOGIES

a) SERIAL SCANNING VERSUS FLOOD EXPOSURE TECHNIQUES

The vat photopolymerization technique can be broadly categorized into two main divisions: serial scanning and flood exposure. In the serial scanning method, which is also widely known as Stereolithography Apparatus (SLA), the machine uses two motors, one for the X and one for the Y axes. These two motors help the light beam from a laser/UV source to aim across a print area to cure the photopolymer resin according to the CAD model. In this method, each layer is divided into a set of points and lines, the coordinates of which are fed to the two motors.

In addition to traditional SLA, two photon polymerization (2PP) is another example of serial scanning techniques, which is developed to improve the resolution and enable printing of micro/nano-scale components. Two-photon absorption (2PA) is a third-order nonlinear optical occurence. If the beam of an ultrafast laser is focused tightly on a particular volume of photocurable material, the polymerization process can be initiated by two-photon absorption within the focal region [Farsari 2009]. The degree of 2PA is directly proportional to the square of incident light intensity and the maximum amount of absorption occurs at the focal point of light. 2PP induced by a near-infrared laser (typically a Titanium Sapphire laser with wavelength around 800 nm) can fabricate arbitrary and highly precise 3D microstructures with high resolution on the nano-scale [Xing 2015].

In the flood exposure technique, which is also widely known as Digital Light Projection (DLP), a digital projector projects a single image of each layer across the entire vat containing the photopolymer resin. Hence, the image of each layer is made of square pixels. The advantage of DLP lies in the fact that it produces large parts quicker than the SLA though it introduces some tradeoffs between resolution and surface finish [Formlabs 2017]. The DLP technology also reduces

the cost of a vat photopolymerization printer by using an ultraviolet lamp as the light source instead of a laser. In the flood exposure techniques the entire vat is exposed at a time to the sliced image of the CAD file projected from the digital light projector. This ensured each layer being cured at once unlike the Serial Scanning techniques. This ensures a faster 'print' than the Serial Scanning techniques. Though the resolution may be compromised when compared to the Serial Scanning techniques.

Mask projected excimer stereolithography (MPExSL) is a flood exposure process that uses excimer laser irradiation to polymerize and crosslink the resin. The term excimer is a short for excited dimer. The uniqueness of this process lies in the fact that excimer lasers produce high powered and well-shaped beams which are unparalleled in terms of industrial reliability among other high-power UV-light sources. Moreover, excimer lasers can have wavelengths spanning the deep-UV to UV range, which offers the flexibility necessary when using different materials for scaffold fabrication. The applied wavelength is very important since it determines the curing (penetration) depth of the laser pulses into the polymer and subsequently the time needed for scaffold production [Zhou 2013].

b) TOP DOWN VERSUS BOTTOM UP APPROACHES

There are two subcategories in both SLA and DLP techniques in terms of how the parts are printed. They are a top down approach and a bottom up approach. The difference between the two is the way the build platform moves after a layer is cured. In the top down approach shown in Figure 1, after a layer is cured, the platform usually moves down in order to spread the liquid photocurable resin in a thin homogeneous layer. A recoating mechanism may be present depending upon the viscosity of the resin. It helps to spread the resin on the surface. It is particularly useful when the viscosity of the resin is higher (> 3 Pa. s).

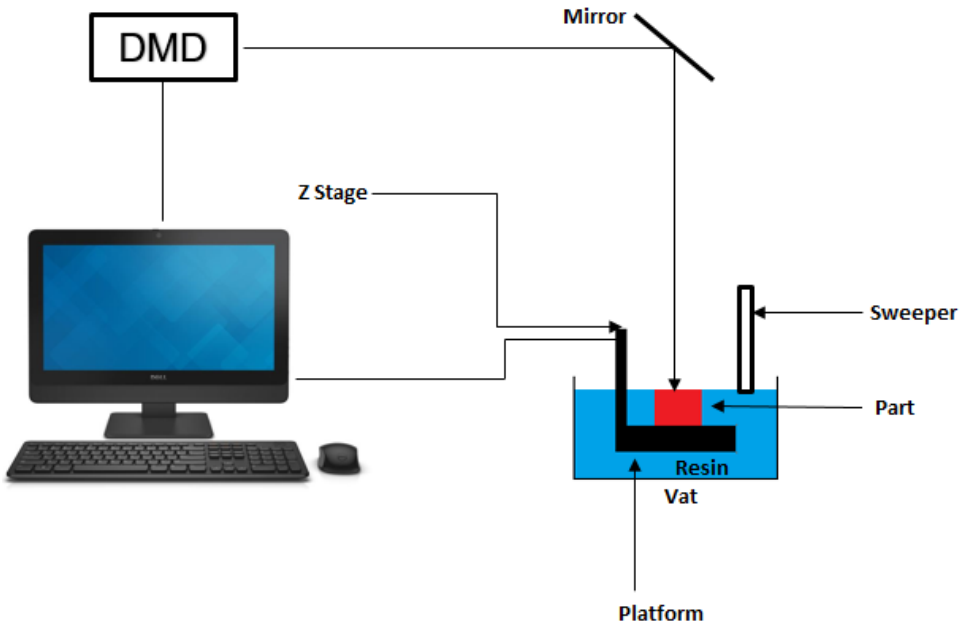

Figure 1: Schematic of the top down vat photopolymerization process

In the bottom up approach shown in Figure 2, the print head descends towards the vat containing the suspension and stops at a point when the distance between the print head and the vat is equal to the predefined layer thickness. At this point, an image is projected by the ultraviolet light engine, according to the CAD model, on the first layer of the suspension, hence curing the complete layer at once. Subsequent to the curing and sticking of the first layer on the metallic print head, the print head ascends by a layer height and a fresh layer of the suspension recoats the space underneath the first layer. After a short interval of exposure, the freshly recoated layer is cured and adhered to the first layer. This process continues till the complete green part is built.

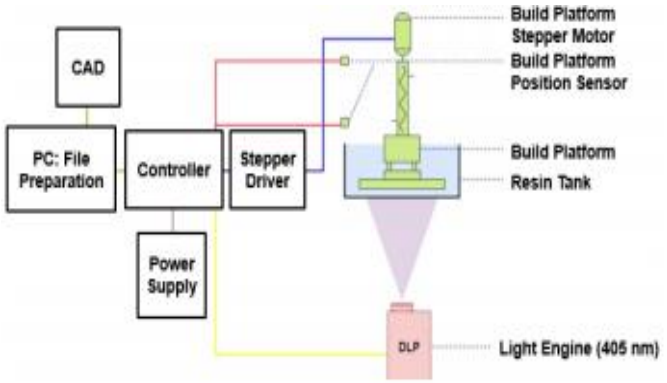

Figure 2: Schematic of the bottom up vat photopolymerization process

The advantages of the bottom up process are:

I. Less resin is needed because the height of the resin vat just needs to be greater than the layer thickness.
II. No sweeping mechanism is required.
III. The absence of oxygen accelerates the curing process of the liquid resin.

However, there are certain limitations to the bottom up approach as well. One of the most limiting disadvantage is the fact that the cured layer may stick to the vat instead of sticking to the print head. There are some remedies suggested in the literature for this problem such as:

I. Increase the exposure on the individual layers so that they may stick to the print head or previous layers.
II. Coating the vat with a layer of polymer such as Teflon to reduce the attachment force of the cured layer on the vat.
III. By oxygenating a permeable layer just below the part being printed, continuous printing without the need of peeling process is ensured. This technology is patented by Carbon3D.

CHAPTER III

POLYMER/CERAMIC COMPOSITE POWDER FOR INDIRECT POWDER BED FUSION

3.1 MATERIALS

For the preparation of composite alumina microspheres, alumina powder of 0.3 μm (Allied High Tech Products, Inc., USA), polyamide (Nylon 12) (Goodfellow Cambridge Limited, USA), and Dimethyl sulfoxide (Sigma Aldrich, USA) were used.

3.2 EXPERIMENTAL METHODS

The research on additive manufacturing (AM) of ceramics gained impetus in the early 1990s but is still in its nascent stages [Shahzad 2013]. Ceramic materials have unique properties and these properties can be leveraged in a myriad of diverse applications. The need for AM of ceramics was felt due to severe limitations involved in their machining, which include, but are not limited to, potential surface damage, small material removal rate, high tool wear rates, long machining times etc. AM can be broadly categorized into seven principal categories [König 1991]. One of them is the powder bed fusion process. Selective laser sintering (SLS) is the commercial term for processes which work on the powder bed fusion principle. SLS can be further categorized into direct and indirect processes [ASTM 2012]. Indirect SLS has been explored extensively for 3D printing of ceramic materials [Chakravarthy 2010, Deckers 2016, Shahzad 2013, Goodridge 2007, Kolam 2011, Guo 2013, Subramanian 1995, Liu 2012]. Figure 3 shows the schematics of indirect SLS. Indirect SLS is carried out in four steps. In the first step, a composite powder containing a ceramic material and a binder is prepared. In the second step, a ‘green part’ is produced by laser processing of the composite powder. In this step the binder melts and binds the ceramic particles. In the third

step, the ‘green part’ is de-bound to form a ‘brown part’. In the last step, the brown part is sintered and further densified to form the sintered specimen. Densification techniques (isostatic pressing, infiltration, etc.) can be used to further increase the density of the part [Deckers 2012].

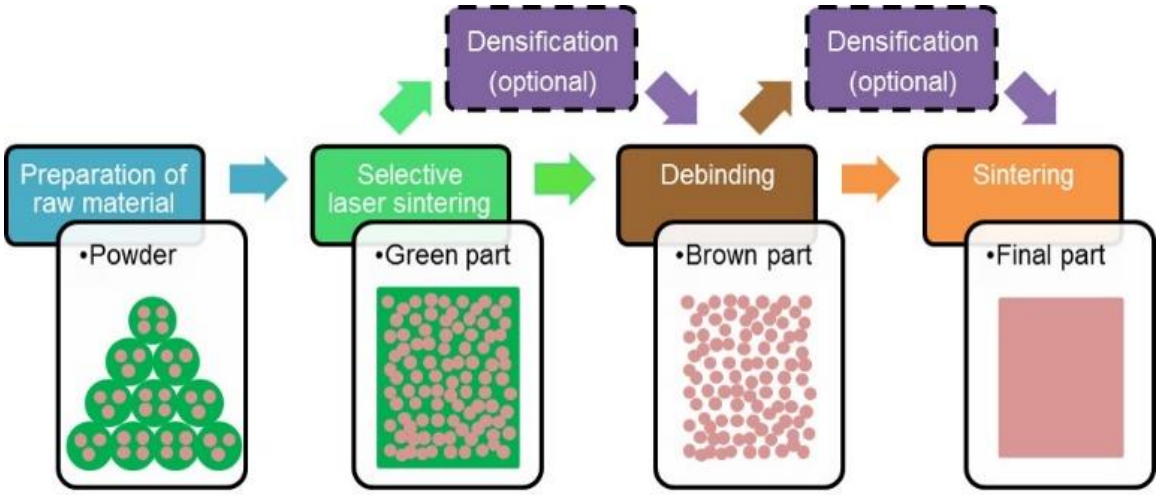

Figure 3: Schematic of indirect selective laser sintering for preparing ceramic parts

The feasibility of using this method to manufacture ceramic parts has been demonstrated on various ceramic materials [Chakravarthy 2010, Deckers 2016, Shahzad 2013, Goodridge 2007, Kolam 2011, Guo 2013, Subramanian 1995, Liu 2012]. However, the flowability and sinterability of powder are rarely studied, although they are critical powder characteristics that determine the properties of printed and sintered ceramic materials. The main objective of this study is to study the effect of the binder fraction on the flowability and sinterability of the composite powder. Reported methods to produce composite powders for indirect SLS include ball milling [Liu 2012] and thermally induced phase separation (TIPS) [Shahzad 2013]. The composite particles from ball milling are irregular in shape, showing inferior flowability and deposition quality. TIPS has been

demonstrated to produce spherical composite particles with controllable sizes [Shahzad 2013] and thus is used in this study.

3.2.1 POWDER PREPARATION

A process known as thermally induced phase separation (TIPS) was employed to produce the composite microspheres [Deckers 2012]. Figure.4 shows the schematic of the TIPS process. Polyamide (Nylon 12) (Goodfellow Cambridge Limited, USA) and de-agglomerated alumina powder with a mean particle size of 0.3 μm (Allied High Tech Products, Inc., USA) were mixed by three volume ratios (20:80, 50:50, and 60:40) in dimethyl sulfoxide (DMSO). The mixture was then mechanical stirred at 300 rpm and heated to ~135˚C under the inert atmosphere of argon to prevent chemical reactions of flammable DMSO. The mixture was naturally cooled to room temperature to allow polyamide to precipitate and engulf the alumina particles. Vacuum filtration was then employed to separate the composite microspheres from DMSO. The filtrate was then washed multiple times using pure ethyl alcohol to completely remove the DMSO. These particles were then dried and filtered using a 90-μm sieve.

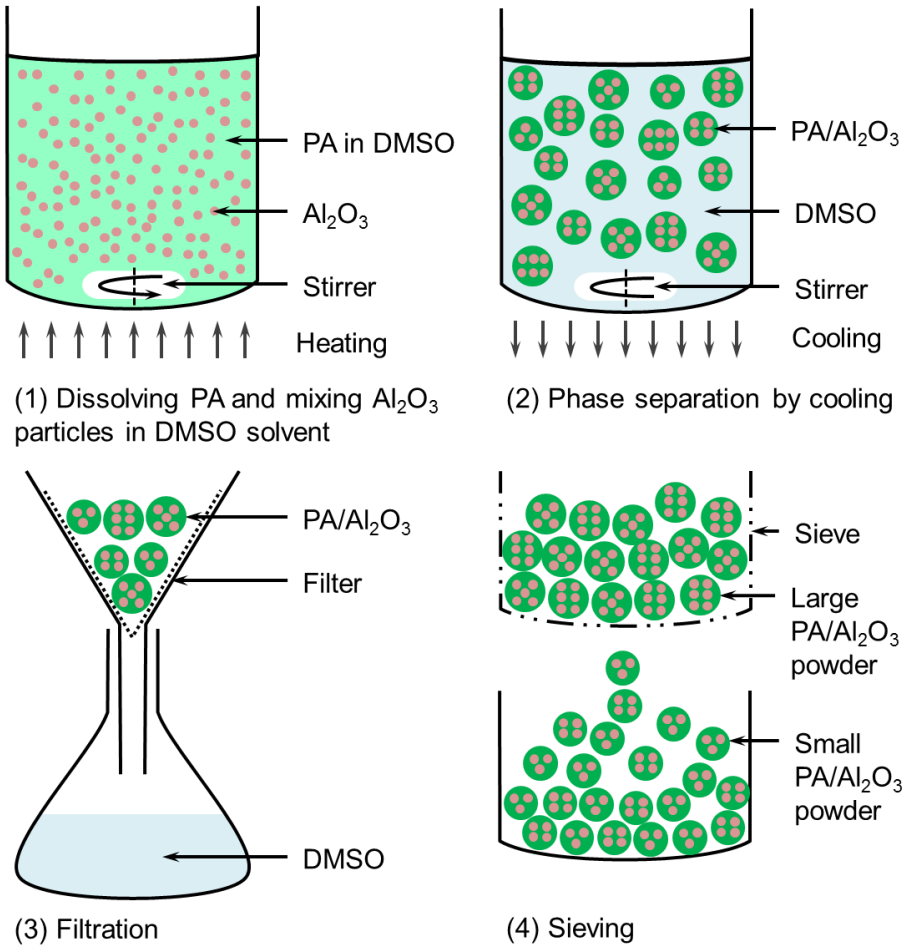

Figure 4: Schematic of the powder preparation using thermally induced phase separation

3.2.2 MICROSTRUCTURAL STUDY

The size and morphology of the composite powders determine the flowability and sinterability of the powders and thus were studied using Scanning Electron Microscope (SEM, TESCAN VEGA II LSU, BrnoKohoutovice, Czech).

3.2.3 MEASUREMENT OF FLOWABILITY

Flowability is the ease with which the powder can flow under a set of given conditions. Presently, there is no universal model which can be used to forecast the flowability of a powder under any given conditions [Prescott 2000]. Flowability depends on a combination of complex parameters

such as the material characteristics and material handling equipment. One of the most widely accepted theories which contribute to the flowability of the powders is the presence of electrostatic force and the Van der Waals force among the powder particles. As the particle size increases, the cohesive forces decrease and consequently the flowability increases.

There are various acceptable methods to measure the flowability, which include Hausner ratio and Carr index, angle of repose, shear cell testing, and relative packing density. In this study, the relative packing density was used to compare the flowability of the different powders produced due to the simplicity of the method. The packing density of the powder was determined by measuring the masses of the powder and water that occupy the same volume. The mass measurements were conducted using an analytical balance (Torbal AGCN200) with an accuracy of 0.1 mg. The packing density of the powder (ρ_p) is given by

$$\rho_p = \frac{\rho_w m_p}{m_w}$$

where ρ_w is the density of water at the measurement temperature, and m_p and m_w are the masses of the powder and water, respectively. The relative packing density (ρ') is given by

$$\rho_p' = \frac{\rho_p}{\rho_{th}}$$

where ρ_{th} is the theoretical density of the powder material, i.e., alumina in this study.

3.2.4 MEASUREMENT OF SINTERABILITY

Sintering is defined as "a thermal treatment for bonding particles into a coherent, predominantly solid structure via mass transport events that often occur on the atomic scale" [German 2014]. The relative density of the solid state sintered specimen is a good measure of its sinterability. The effect of the flowability of the powder was blocked in our study by using uniaxial pressing method to

prepare the disc shaped specimen. The thermal processing of the disc shaped specimen was done in a high temperature furnace (KSL-1700X-A2-UL, MTI Corporation, CA) under an air atmosphere which consisted of two steps: de-binding and sintering. The de-binding of the specimen was done by heating the specimen in air up to 600˚C at 1˚C/min and dwelling for 2 hours at 600˚C. This ensured the removal of the polyamide by thermal decomposition. The sintering of the parts followed immediately after the de-binding. The specimen was heated up to 1600˚C at 5˚C/min and dwelled at 1600˚C for an hour before furnace cooling to room temperature. The Archimedes' method was then used to measure the density of the sintered specimen. Firstly, the mass of a specimen was measured in the air, which is called the dry mass (m_d). The specimen was then suspended in water to determine its wet mass (m_w), which is the dry weight minus the buoyancy from water. The mass measurements were conducted using the same analytical balance (Torbal AGCN200). The dry and wet masses were finally used to calculate the density of the specimen (ρ_s) by the following formula,

$$\rho_s = \rho_{wt} \frac{m_d}{m_d - m_w}$$

The sinterability is described using the relative sintered density of the specimen,

$$\rho_s' = \frac{\rho_s}{\rho_{th}}$$

Three specimens were prepared from each powder to gauge the uncertainty of the measurements.

3.3 RESULTS AND DISCUSSION

SEM images of the three powders prepared are shown in Figure 5. It shows that the shape of the produced particles under all of the three conditions are nearly spherical. From Figure 5, it could also be inferred that the size of the composite microspheres increased as the fraction of the

polyamide to alumina increased from 20 to 60 vol. %. The sizes of the composite microspheres with the polyamide-to-alumina ratios of 20:80, 50:50, and 60:40 were found to be in the range of 10-20 μm, 20-25 μm, and 30-60 μm, respectively. This increase in size with the increase in the fraction of the polyamide could be attributed to the fact that the nucleation and growth rate of polyamide increased due to the increased concentration of polyamide in the solution.

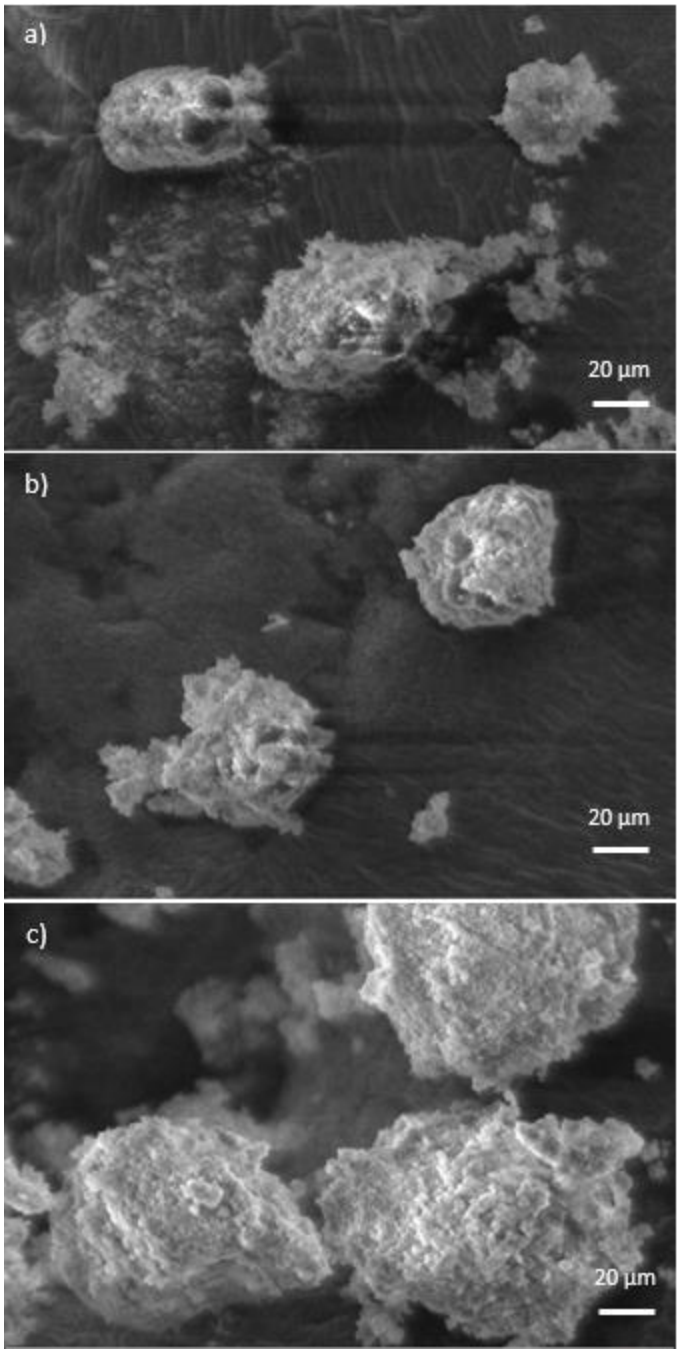

Figure 5: Particle morphology of composite particles at different polyamide-to-alumina ratios: a) 20:80, b) 50:50, and c) 60:40

3.3.1 FLOWABILITY

Figure 6(a) shows the dependence of the relative packing density of composite powder on the fraction of polyamide. As the fraction of the polyamide in the composite powder increased, the relative packing density increased, suggesting that the flowability increased. As the polyamide fraction increased, the composite particle size increased, which made the gravitational force more significant than the electrostatic force and the Van der Waals force. The dominance of the gravitational force helped the particles contact each other better, thereby occupying less space. In addition, the reduction of the electrostatic force and the Van der Waals force also decreased the friction between particles, thereby helping the particles fill in the space between each other.

3.3.2 SINTERABILITY

Figure 6(b) shows the effect of the polyamide fraction on the relative sintered density. As the fraction of the polyamide in the composite increased, the density of the specimen decreased. It is a well-documented fact that the gaseous products exit the sample being de-bound by diffusion and permeation. The dominance of the diffusion or permeation depends upon the size of the pores, pressure, and molecular weight [German 1987]. The samples with higher polyamide fraction required a lower de-binding rate and consequently a longer de-binding time to get completely de-bound. As the same rate of de-binding was used for all the samples, a part of de-binding could have occurred during the sintering process, causing turbulent flow of gases out of the samples. This may have produced higher porosities in the samples. Hence, for the samples with the higher polyamide fraction, sintering could not be completed, accounting for the low resultant sintered density.

Fig. 7 shows the SEM images of the discs prepared using the different composite powders (polyamide-to-alumina ratios of 20:80, 50:50 and 60:40). As can be seen from Fig. 7(a), there are

a number of pores on the surface of the disc with 20% polyamide but no cracks. Fig. 7(b) and 7(c) shows the surface of the disc with 50% polyamide at a low and high magnification, respectively. It can be clearly seen that the specimen has wide cracks on its surface. Fig. 7(d) shows the surface of the disc with 60% polyamide at a high magnification. The SEM images support the observed relationship between the polyamide fraction and the sinterability: as the fraction of the polyamide increases in the specimen, so does the size of cracks on the surface of the specimen, consequently increasing the porosity and decreasing the sintered density.

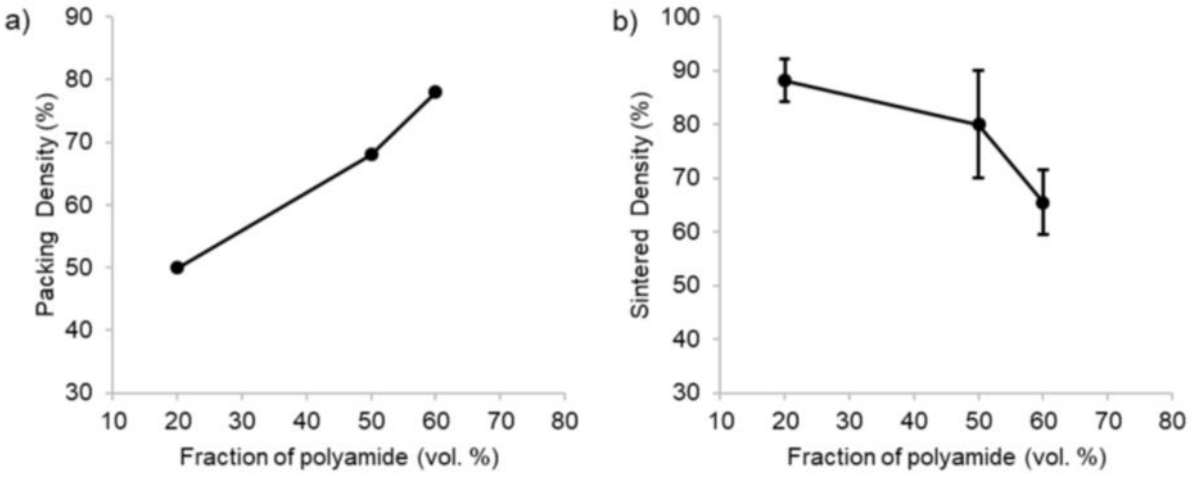

Figure 6: Effects of the fraction of polyamide on a) powder packing density and b) sintered density

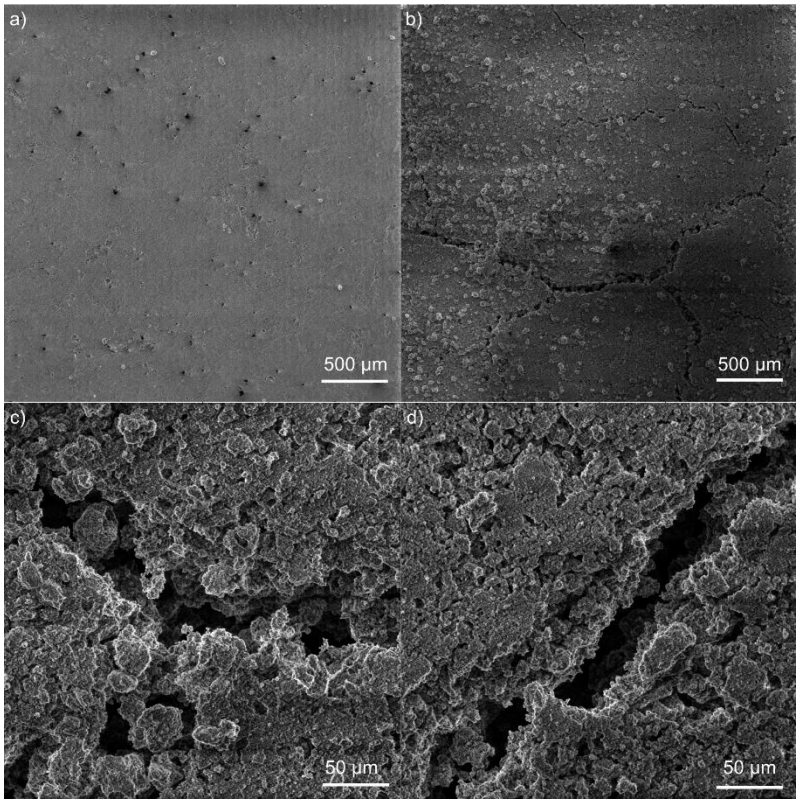

Figure 7: SEM images of disc specimens with 20% polyamide at a low magnification a), 50% polyamide at a low b) and high c) magnification, and d) with 60% polyamide at a high magnification

3.4 SUMMARY

The TIPS method was used to produce nearly spherical polyamide/alumina particles with DMSO as an organic solvent. The size of the composite particles increased as the polyamide fraction increased. The flowability of the composite powder was found to increase with the increase in the polyamide fraction while the sinterability was found to decrease with increase in the polyamide fraction. Since flowability and sinterability are both important factors to produce a high-quality part using indirect SLS, it is important to maintain the balance between the two parameters by carefully controlling the fraction of binder in a binder/ceramic composite due to its contradictory effects on the two factors.

CHAPTER IV

CERAMIC SUSPENSION FOR VAT PHOTOPOLYMERIZATION USING COMMERCIAL PHOTOPOLYMERIZABLE RESIN

4.1 MATERIALS

For the preparation of the ceramic loaded photopolymerizable resin suspension, alumina powder of 0.3 μm (Allied High Tech Products, Inc., USA) was used. Multipurpose resin (XYZprinting) was used as the photopolymerizable resin

4.2 EXPERIMENTAL METHODS

4.2.1 SUSPENSION PREPARATION

The suspension was prepared by adding 10 vol. % of alumina to the photopolymerizable resin. The suspension was then stirred mechanically at 200 RPM in a beaker of 50 mL for 30 minutes in the dark at room temperature to prevent the photopolymerization of the resin.

4.2.2 VAT PHOTOPOLYMERIZATION

The vat photopolymerization 3D printer (Figure 8) used for this study is Nobel Superfine from XYZprinting, Inc., USA. It has a maximum build volume of $64 \times 40 \times 120$ mm^3 (W × D × H) and a resolution of 25~100 μm in the Z-direction and 50 μm in the X/Y direction.

The printer shown in Figure 8 is based on the digital light processing (DLP) technology. The DLP technology exposes each layer at once with an image projected by a digital projector according to the CAD model [Hatzenbichler 2012]. This flood exposure has the advantage of rapid manufacturing. The DLP technology also reduces the cost of a vat photopolymerization printer by using an ultraviolet lamp as the light source instead of a laser.

After the preparation of the suspension, it was transferred to the vat on the printer. After the printing operation was started, the metallic print head descended towards the vat containing the suspension and stopped at a point when the distance between the print head and the vat was equal to the predefined layer thickness, 50 µm in this study. At this point, an image was projected by the ultraviolet light (405 nm) engine, according to the CAD model, on the first layer of the suspension, hence curing the complete layer at once. Subsequent to the curing and sticking of the first layer on the metallic print head, the print head ascended by a layer height and a fresh layer of the suspension recoated the space underneath the first layer. After a short interval of exposure, the freshly recoated layer was cured and adhered to the first layer. This process continued till the complete green part was built. The printed green ceramic body was a polymer matrix composite containing alumina particles. Cubic green ceramic body of different sizes (5 mm, 10 mm, 15 mm, and 20 mm) were printed.

Figure 8: Front, back and side view of the Nobel Superfine printer

4.2.3 DE-BINDING AND SINTERING

After the formation of the green ceramic body the thermal processing was performed in a high-temperature furnace (KSL-1700X-A2-UL, MTI Corporation, CA) under an air atmosphere, which consisted of two steps: de-binding and sintering. In the de-binding stage, the polymer was removed from the green body by heating to 350˚C at 5˚C/min and then from 350˚ to 550˚C at 1˚C/min. The sintering of the parts followed immediately after the de-binding. The samples were heated from 550˚C to 1600˚C at 5˚C/min and then dwelled for 1 hour at 1600˚C and then allowed to cool to the room temperature naturally in the furnace. The de-binding and sintering process were combined into a single process. The de-binding and sintering profile is shown in Figure 9.

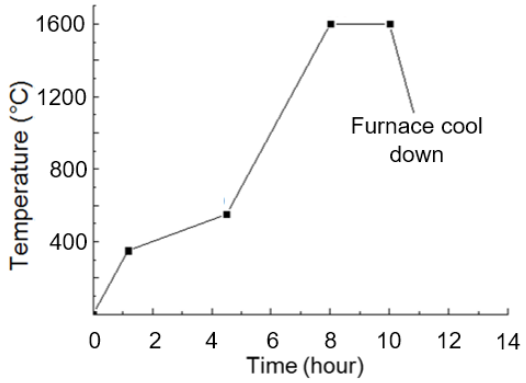

Figure 9: The de-binding and sintering profile for printed cubes

4.2.4 DENSITY MEASUREMENT AND POROSITY ESTIMATION

Density of the sintered samples was measured with Archimedes' method. After the dry mass (m_d) of a sample was measured, the sample was carefully lowered onto a pan suspended in a beaker of deionized water to determine its wet mass (m_w). The mass measurements were done using an

analytical balance (AGCN200, Torbal, NY) with an accuracy of 0.1 mg. The dry and wet masses were then used to calculate the density with the knowledge of density of water as follows,

$$\rho_a = \rho_{wt} \frac{m_d}{m_d - m_w}$$

where ρ_a and ρ_{wt} are the apparent solid density of the sample and the density of water at the experimental temperature, respectively. If a sample has open pores, the water infiltrates the sample and thus the above method measures the apparent solid density that only accounts for the closed pores. In order to obtain the geometric bulk density that accounts for both the closed and the open pores, the samples were coated with an extremely thin layer of wax to eliminate the water infiltration and the aforementioned procedure was repeated. In this case, the geometric bulk density (ρ_g) of the samples was calculated as follows,

$$\rho_g = \rho_{wt} \frac{m_d}{m_d - m_{wc}}$$

where m_{wc} is the mass of the wax coated sample in water. Using these two densities it is possible to calculate the fractions of the total, open and closed pores present in the samples. The total porosity (p_t) is calculated as follows,

$$p_t = 1 - \frac{\rho_g}{\rho_{th}}$$

where ρ_{th} is the theoretical density of the material. The closed porosity (p_c) is calculated as follows,

$$p_c = 1 - \frac{\rho_a}{\rho_{th}}$$

The open porosity (p_o) is calculated as follows,

$$p_o = p_t - p_c$$

4.2.5 COMPRESSIVE STRENGTH MEASUREMENT

The compressive strength of the 5, 10, 15 and 20 mm sized cubes were measured using a Universal Mechanical Testing Machine (United Testing STM-100 KN, California, USA).

4.3 RESULTS AND DISCUSSION

A micrograph of the raw alumina particles is shown in Figure 10, which was obtained using a field emission scanning electron microscope (JEOL JSM-7500F). The size of raw alumina particles is actually around 100 nm while the vendor claims 300 nm. An aggregation tendency can be observed.

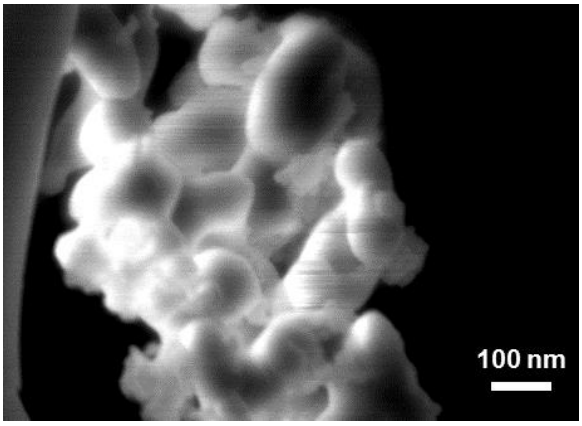

Figure 10: The morphology of the raw alumina particles

The average geometric bulk and apparent solid sintered densities of cubic samples as functions of the green body size are shown in Figure 11. The apparent solid density is measured by taking into consideration the volume of the solid material including the closed pores, whereas the geometric bulk density is measured by considering all the porosity, accessible and inaccessible from the

surface [Jo 2013]. As can be seen from Figure 11, the geometric bulk density for the 5-mm cube was the largest among all samples. A gradual decrease was observed as the size of the sample increased from 5 mm to 15 mm, after which it remained constant. A similar trend was observed in the case of the average apparent solid density, where the apparent solid density for the 5-mm cube was the largest among all samples. There was a decrease as the part size increased from 5 mm to 10 mm, after which it became constant. There is a direct relationship between the apparent solid and geometric bulk densities and the volume of porosities in the samples which can be explained by the variation of porosity generation with the increase in the part size.

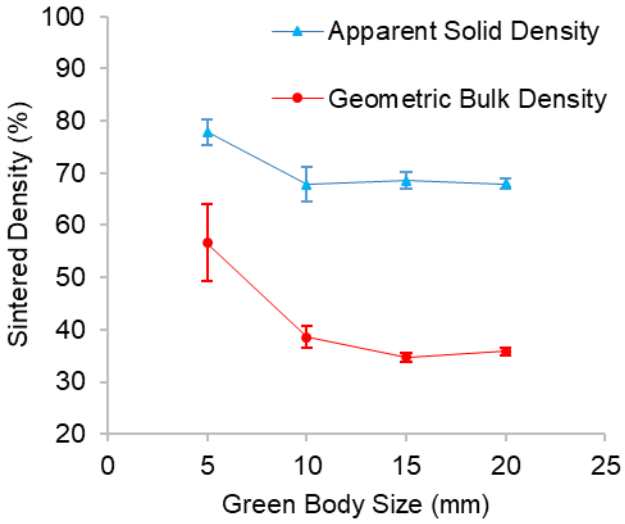

Figure 11: Effect of green body size on sintered density

The total, open and the closed porosities were calculated and plotted against the green body size and are shown in Figure 12. The open porosity as well as the closed porosity increase as the part size increases and so does the total porosity. This can be explained by the de-binding and sintering

behaviors of the samples. Since the total porosity is the sum of the open and closed porosities, it follows the same trend as those.

It is a well-documented fact that the gaseous products exit the sample being de-bound by diffusion and permeation. The dominance of the diffusion or permeation depends upon the size of the pores, pressure, and molecular weight [German 1987]. The time (t) taken for the gaseous products to move to the surface is given

$$t = kL^2$$

where k is a proportional constant and L is the size of a sample. It could be concluded that larger the size of the sample longer the time taken for the gaseous substances to reach the surface. Since the same temperature profile was used to de-bind and sinter all the samples, this might have resulted in varying degree of binder removal from the differently sized samples during de-binding. During the sintering cycle which followed the de-binding cycle, a higher ramp rate of 5˚C/min was used which could cause any residual binder in the larger samples to decompose and flow out of the sample in a turbulent manner, thereby generating more pores and cracks. It can be seen from Figure 6 that the curve for both open and closed porosities follow an almost similar trend. Both gradually increased as the size of the cubes increased. This could be explained by the fact that the degree of de-binding decreased during the de-binding cycle and more residual binder was left behind in the cubes as the cube size increased. This meant that bigger the cube size, more turbulent the outward flow of the gaseous products was during the sintering cycle, thereby causing bigger pores and cracks to be formed inside the cubes as well as on the surface.

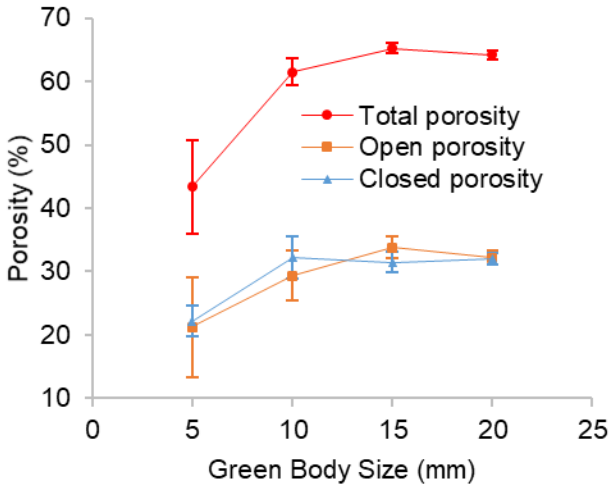

Figure 12: Effect of green body size on porosity

Figure 13 shows the stress-strain curve for 5, 10, 15 and 20 mm cubes. It can be clearly seen that the first jag occurs in the red line around 1.2 MPa which indicates the first fracture or failure in the part. The jaggedness in the curves for 10, 15 and 20 mm is well below the compressive stress value of 1.2 MPa, which indicates that fracture occurred in these cubes before reaching a compressive stress of 1.2 MPa. This shows that the compressive strength of the 5-mm cube is greater than those of the 10, 15 and 20 mm owing to the fact that the porosity fraction is the lowest in the 5-mm cube. This underlines the fact that the compressive strength of a part decreases as the fraction of porosity in the alumina part increases.

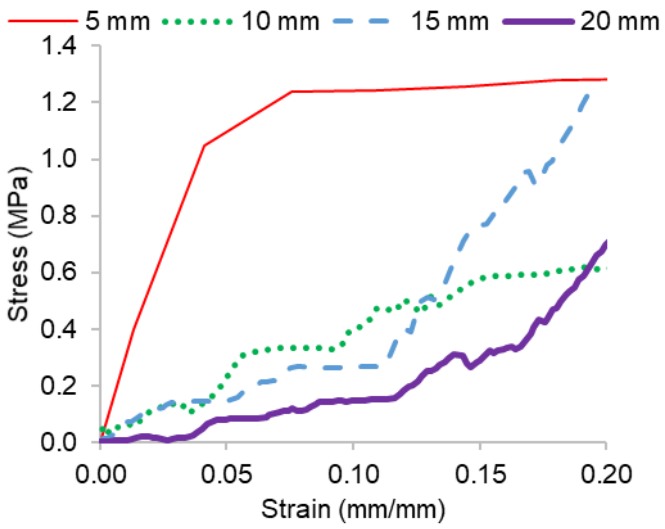

Figure 13: Compressive stress as a function of strain

4.4 SUMMARY

Alumina powder was mechanically mixed into a photopolymerizable resin. Using this suspension, ceramic green bodies of four sizes (5, 10, 15, and 20 mm) were printed out using a vat photopolymerization printer. The effects of the green body size on the sintered density, porosity and compressive strength were studied. The properties of the ceramic parts produced by the vat photopolymerization were found sensitive to the part size. The 5-mm cube achieved the highest density, lowest porosity, and highest compressive strength. This work demonstrated that porous ceramic structures can be produced by vat photopolymerization using a low loading of ceramic particles in a photopolymerizable resin. Future work includes optimizing the de-binding rate for each size of the green body, increasing the loading of the ceramic in the resin and studying the variation of the sintered density by using different photopolymerizable resins for the preparation of the ceramic-resin suspension.

CHAPTER V

CERAMIC SUSPENSION FOR VAT PHOTOPOLYMERIZATION USING IN-HOUSE PHOTOPOLYMERIZABLE RESIN

5.1 MATERIALS

For the preparation of the ceramic loaded photopolymerizable resin suspension, three different sizes of alumina powders, 0.3 µm (Allied High Tech Products, Inc., USA), 0.5 µm and 0.8 µm (US Research Nanomaterials, Inc., USA), were used. 1, 6 Hexanediol diacrylate (HDDA) (Sigma-Aldrich, USA) was used as the monomer. Oleic acid (Sigma-Aldrich, USA) was used as the dispersant for the ceramic suspensions. Diphenyl (2, 4, 6-trimethylbenzoyl) phosphine oxide (Sigma-Aldrich, USA) was used as the photoinitiator for the ceramic suspensions.

5.2 EXPERIMENTAL METHODS

5.2.1 SINTERABILITY OF ALUMINA POWDERS

Before preparing any suspension and printing the green bodies using the vat photopolymerization technique, the sinterability of the powders of 0.3 µm, 0.5 µm and 0.8 µm was estimated by density measurement after pressing and sintering. 1 g of each of the powder was pressed under 100 MPa using a die of 12.7 mm in diameter. The pressed discs were sintered at 1600 °C for 12 h in a high-temperature furnace (KSL-1700X-A2-UL, MTI Corporation, CA) under an air atmosphere. The ISO 18754 [ISO 2003] method was then used to measure the density of the sintered specimen. Firstly, the mass of a specimen was measured in the air, which is called the dry mass (m_1). The specimen was then boiled in water for 3 hours and then allowed to cool down to room temperature. The specimen was then suspended in water to determine its wet mass (m_2), which is the dry weight minus the buoyancy force due to water. The wet specimen was then wiped with a wet paper towel

and its mass (m_3) was determined. The mass measurements were conducted using the same analytical balance (Torbal AGCN200). The bulk density was calculated by the following formula,

$$\rho_b = \rho_{wt} \frac{m_1}{m_3 - m_2}$$

The apparent solid density of the specimens was measured using the formula,

$$\rho_s = \rho_{wt} \frac{m_1}{m_1 - m_2}$$

5.2.2 SUSPENSION PREPARATION

Six different suspensions were prepared by adding varied quantities of alumina by volume fraction to the in-house resin which was 1, 6 Hexanediol diacrylate (HDDA) in this case. In the case of monomodal suspensions, after all the alumina powder had been added to the HDDA, the dispersant was added to the suspension. In the case of the bimodal suspensions, the dispersant was added after the primary powder had been added. After the addition of the dispersant, the dopant alumina powder was added to the suspensions. The weight ratio of the dispersant to alumina powder was controlled at 1:1000. The photoinitiator was added to the suspension at the end. The weight ratio of the photoinitiator to HDDA was controlled at 1:100. The suspension was then stirred mechanically at 200 RPM in a beaker of 50 mL for 30 min in the dark at room temperature to prevent the photopolymerization of the resin.

The Figure 14 shows the composition of the six suspensions prepared using the different volume fractions of HDDA and alumina (0.3 µm, 0.5 µm, 0.8 µm). The amount of loading of the alumina powder for all the six suspensions (monomodal and bimodal) was decided for 0.1 wt. % of the dispersant. The various volume fractions of alumina in each case was decided after gauging the suitable flowability of the suspension for the Nobel Superfine printer. In the case of bimodal suspensions, a combination of two alumina powders was added to the photopolymerizable resin to

form the suspension. In each case of the bimodal suspension, 1 vol. % of the larger sized alumina powder was replaced with the finer alumina powder. If the flowability of the ceramic suspension was too poor for the printer the parts did not get printed completely as the suspension could not flow underneath the print head every time it ascended by a layer thickness.

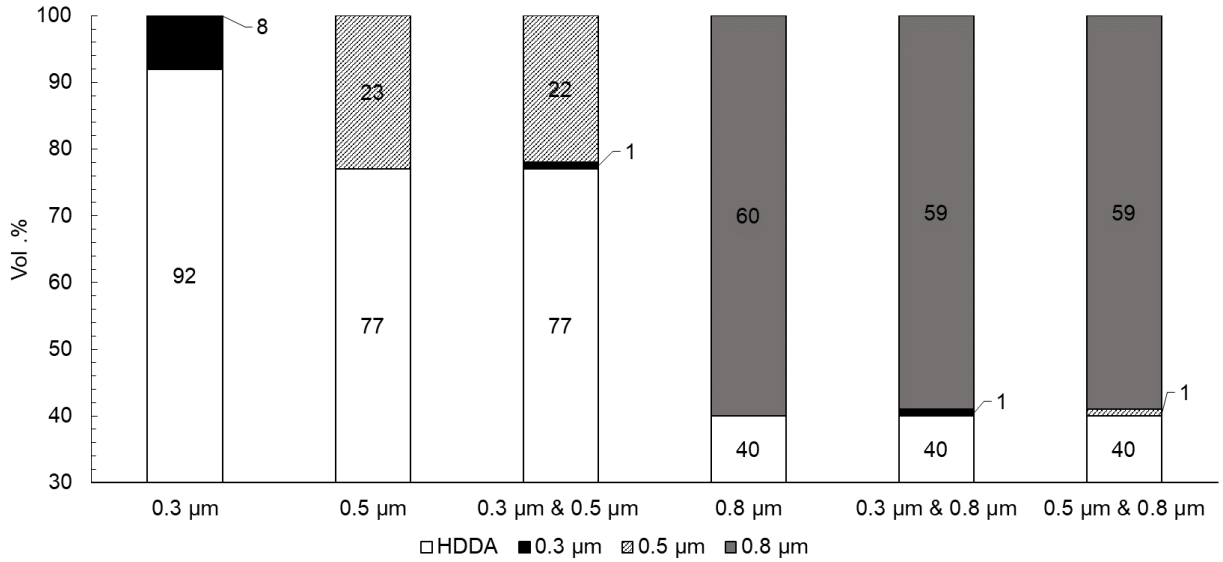

Figure 14: Composition of suspensions

5.2.3 VAT PHOTOPOLYMERIZATION

The vat photopolymerization 3D printer, Nobel Superfine from XYZprinting, Inc., USA, was used to produce disc shaped green bodies of 2 mm in height and 5 mm in diameter. The layer thickness was 50 µm. The exposure parameters that were chosen for the first eight base layers were: a) curing time of 60 s for each layer and b) a power intensity of 52 W/m^2. The exposure parameters that were chosen for the rest of the model layers were: a) curing time of 30 s for each layer and b) a power intensity of 41.6 W/m^2.

5.2.4 DEBINDING AND SINTERING

After the formation of the green ceramic body, the thermal processing was performed in a high-temperature furnace (KSL-1700X-A2-UL, MTI Corporation, CA) under an air atmosphere, which consisted of two steps: debinding and sintering. Figure 15 shows the temperature curve for the debinding and sintering for all the green bodies printed. In the debinding stage, the polymer was removed from the green body by heating to 600˚C at 0.2˚C/min and then dwelling at 600˚C for 8 h. The sintering of the parts followed immediately after the de-binding. The samples were heated from 600˚C to 1600˚C at 5˚C/min and then dwelled for 12 h at 1600˚C and then allowed to naturally cool to the room temperature in the furnace. The temperature range for debinding was chosen owing to the data obtained from the thermogravimetric analysis (TGA). The TGA was done using the SDT Q600 (TA Instruments). The TGA analysis on the samples was done from 50 ˚C to 1400 ˚C at 10 ˚C/min. TGA curve in Figure 16 shows that the maximum amount of weight loss occurred between 350˚C and 550˚C.

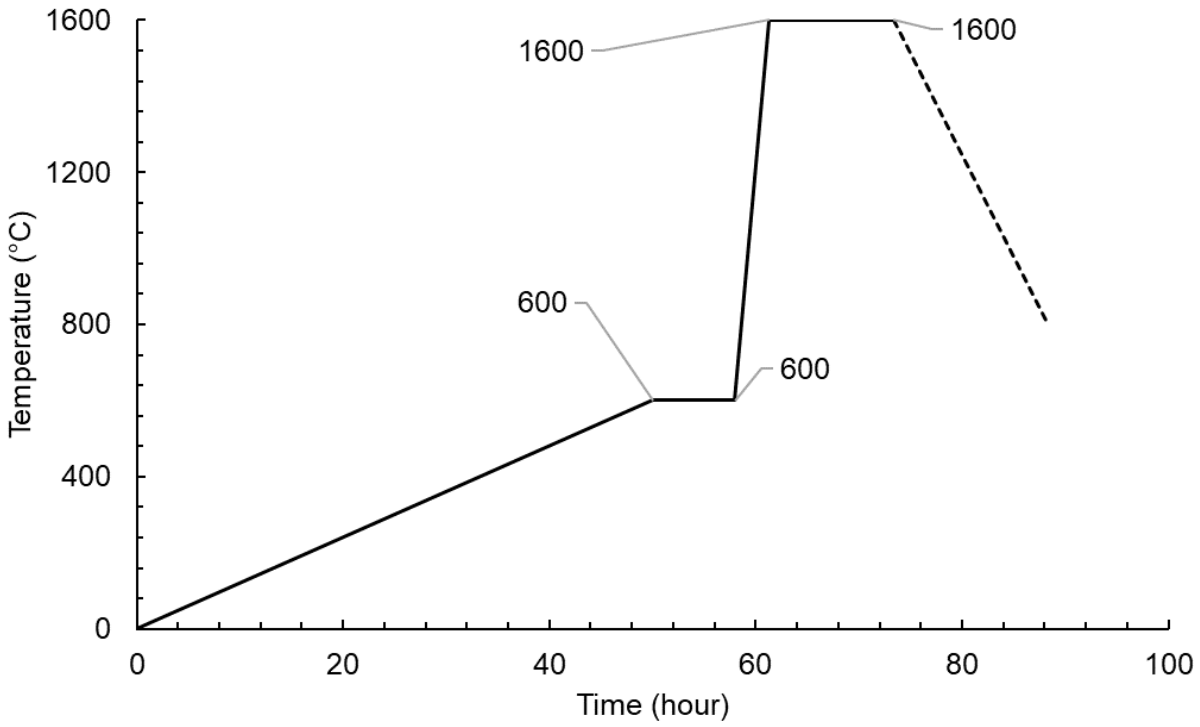

Figure 15: Temperature profile for debinding and sintering

Moreover, the verification of the temperature profile was done by estimating the debinding efficiency in each of the samples given by the following formula,

$$\eta = \frac{\Delta m}{m_0}$$

where, Δm and m_0 denote the mass lost during the thermal post-processing process and the mass of polymer in the printed green bodies, respectively. The weights of the samples before and after debinding and sintering were measured to estimate the amount of binder lost during the debinding process.

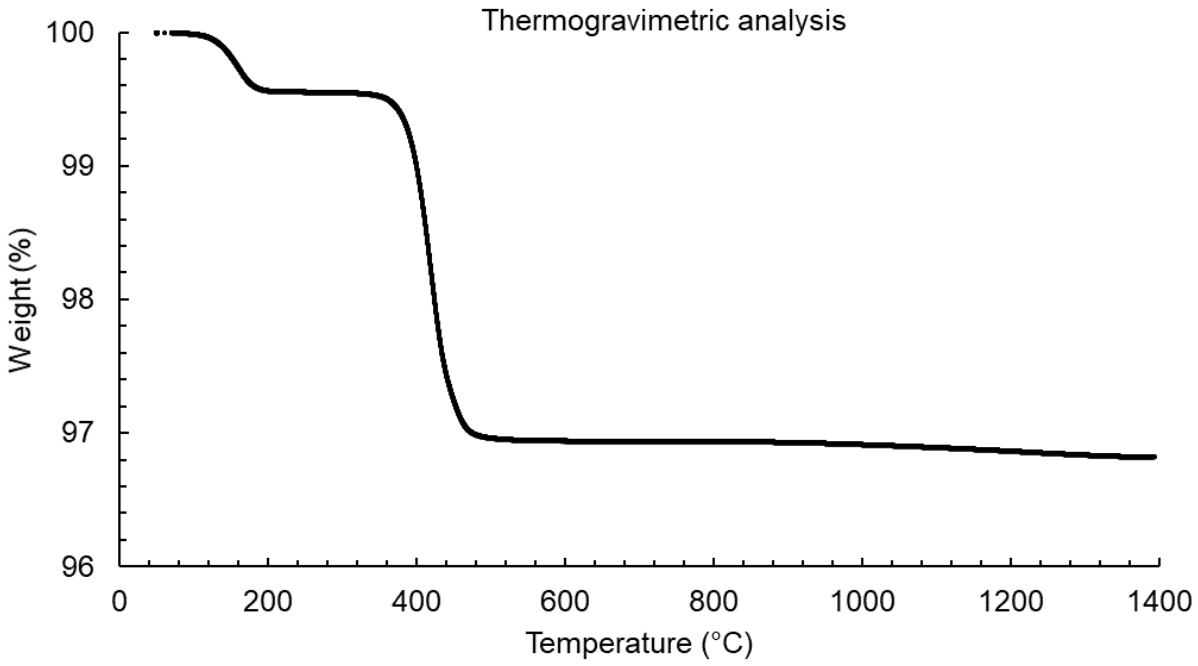

Figure 16: TGA for the printed green bodies with HDDA

5.2.5 DENSITY MEASUREMENT AND POROSITY ESTIMATION

The ISO 18754 method [ISO 2003] was then used to measure the density of the printed and sintered specimen, as described in Section 5.2.1.

Using the apparent solid and the bulk densities, it is possible to calculate the fractions of the total, open and closed pores present in the samples. The total porosity (p_t) is calculated as follows,

$$p_t = 1 - \rho_b'$$

where ρ_{th} is the theoretical density of the material and ρ_b' is the ratio of the bulk density to the theoretical density. The open porosity (p_o) is calculated as follows,

$$p_o = 1 - \frac{\rho_b}{\rho_s}$$

The closed porosity (p_c) is calculated as follows,

$$p_c = \rho_b{}' (1 - \rho_s)/\rho_s$$

5.3 RESULTS AND DISCUSSION

Three different powder particles (0.3 µm, 0.5 µm and 0.8 µm) were pressed and sintered to assess their sinterability. Figure 17 shows the bulk densities of the three pressed and sintered specimens. As seen from Figure 17, the bulk density decreases as the particle size increases. The powder of 0.3 µm achieved a nearly full density. This is attributed to the fact that the particles with the smaller size have higher specific surface energy, hence have better sinterability. As the size of the particles increases, the specific surface energy decreases, hence the sinterability also decreases.

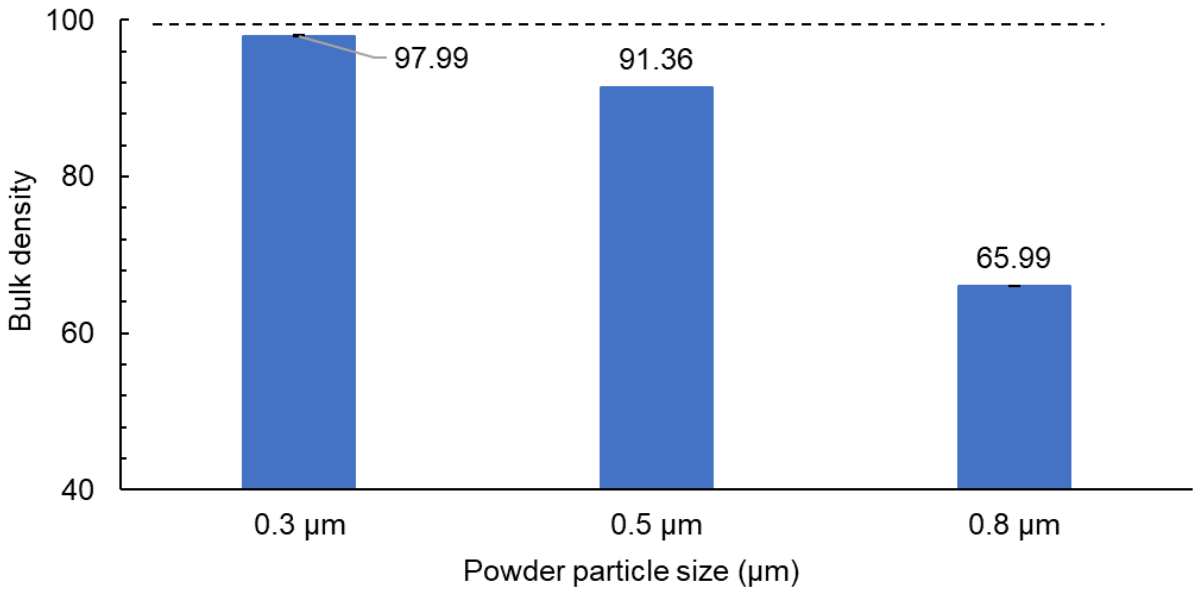

Figure 17: Bulk density of alumina for different sized particles

Figure 18 shows the debinding efficiency for all the samples from the six suspensions investigated. It can be seen that almost complete debinding occurred for all of the samples. The debinding efficiency of more than 100% for some samples could be attributed to weight loss due to handling of the samples.

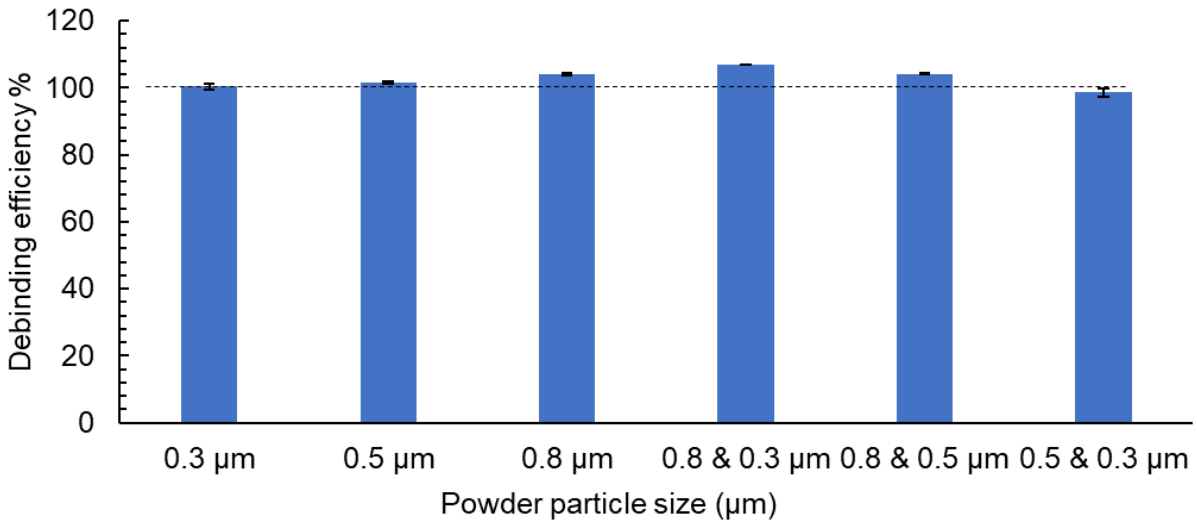

Figure 18: Debinding efficiency for the samples

Figure 19 shows the apparent solid and bulk density of the samples containing the six suspensions. The suspension represented in the first clustered column contained 8 vol.% 0.3 µm, the second contained 23 vol. % 0.5 µm powder particles, the third contained 22 vol. % 0.5 µm along with 1 vol. % 0.3 µm particles, the fourth contained 60 vol. % 0.8 µm particles, the fifth contained 59 vol. % 0.8 µm along with 1 vol. % 0.3 µm particles and the sixth contained 59 vol. % 0.8 µm along with 1 vol. % 0.5 µm particle. The second box circumscribing the column charts shows the comparison of the apparent solid density and bulk density between the three samples (0.8 µm, 0.3 µm & 0.8 µm, and 0.5 µm & 0.8 µm). As can be seen from the figure, the bulk density of the

sample containing the 0.3 µm & 0.8 µm particles is the highest, that of 0.5 µm & 0.8 µm particles being the second highest, and that of the 0.8 µm particles being the lowest. This can be attributed to the fact that even a small loading (1 vol.%) of 0.3 µm sized particles as dopant to the 0.8 µm particles is effective as it increased the overall bulk density of the sintered samples. Similarly, there was an increase in the bulk density of the 0.8 µm particles when 0.5 µm particles were added as a dopant. The first box circumscribing the column charts shows the comparison of the apparent solid density and geometric bulk density between the two samples (0.5 µm and 0.3 µm & 0.5). A trend similar to the one seen in the second box can be seen here as well, though it is not as pronounced in this case.

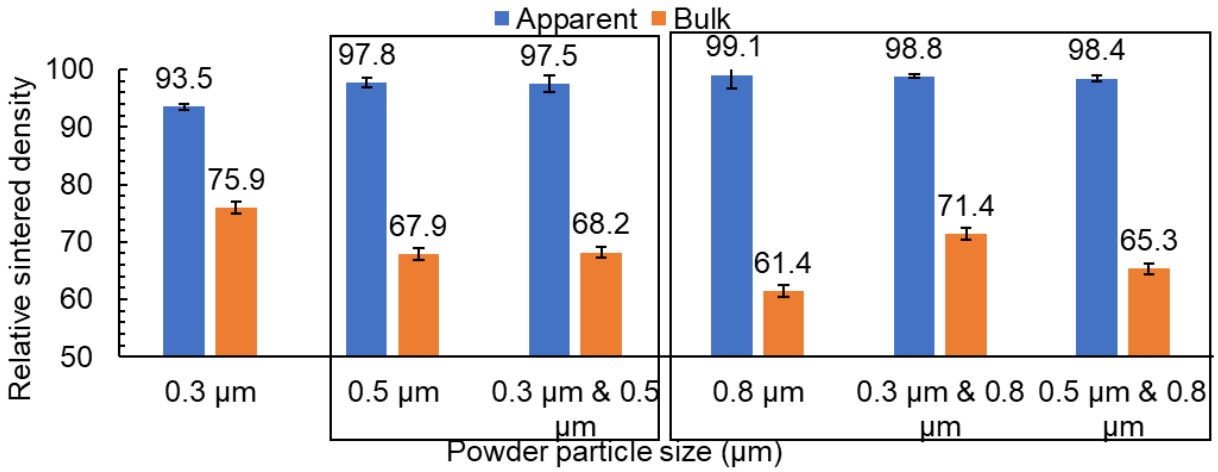

Figure 19: Apparent solid and bulk density of the samples

It can also be seen from Figure 19 that the bulk density of the specimen containing the 0.3 µm powder was the highest among the specimen with monomodal loading even when the loading of the 0.3 µm powder was the lowest (8 vol.%). This can be attributed to the fact that the sinterability of the finest powder was the best when compared to 0.5 µm and 0.8 µm powders. The bulk density

of the 0.8 µm powders is the lowest among the monomodal suspensions and the bulk density of the 0.5 µm powders lies between the bulk densities of the 0.3 µm and 0.8 µm powder.

Figure 20 shows the open and closed porosities for the six sintered samples. As can be observed from Figure 20, the open porosity in 0.3 µm & 0.8 µm particle sintered part is the lowest when compared to the 0.8 µm particle sintered part and the 0.5 µm & 0.8 µm particle part. This is due to the fact that the sinterability of the 0.3 µm & 0.8 µm particles is the best among the three. The same trend can be observed in the 0.5 µm and 0.3 µm & 0.5 µm particle sintered part. The open porosity of the 0.3 µm & 0.5 µm particle sintered part is lesser than the open porosity in the 0.5 µm particle sintered part because the sinterability of the 0.3 µm & 0.5 µm particles is slightly better. The open porosity of the parts just before sintering is the highest to begin with as a lot of voids in the 3D structure just after debinding are still open to the atmosphere. As sintering happens, progressive necking of individual powder particles with each other happens and the open pores start decreasing.

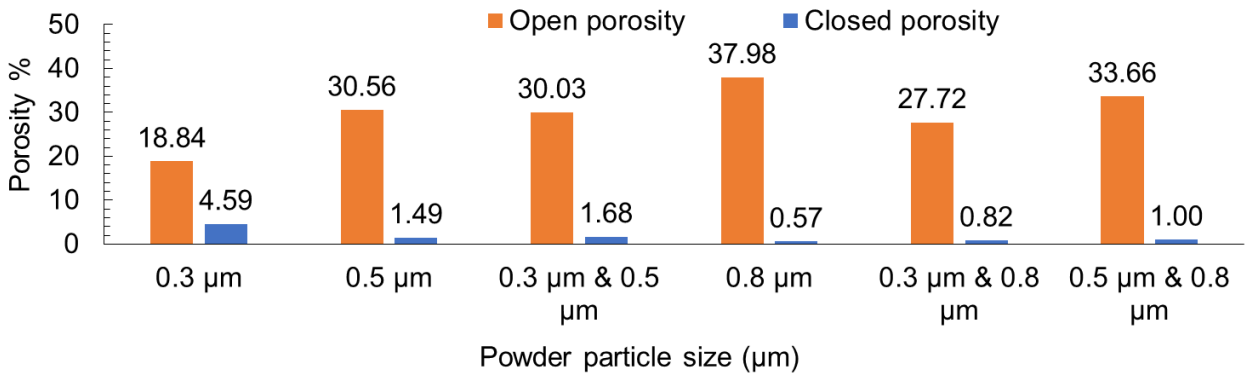

Figure 20: Shows the open and closed porosities for the six sintered samples

SEM images of two printed and sintered specimen, the first containing 0.8 µm particles and the second containing the 0.3 µm & 0.8 µm particles, were taken. Figure 21 and Figure 22 show the SEM images of the specimens containing the 0.8 µm particle and 0.3 µm & 0.8 µm particles respectively. The part with 0.8 µm particles contained 60 vol. % of the 0.8 µm particles. The part with 0.3 µm & 0.8 µm particles contained 1 vol. % of 0.3 µm particles and 59 vol. % of the 0.8 µm particles. It can be clearly seen from the two micrographs that there is a marked change in the particle morphology. The printed and sintered sample from 0.3 µm & 0.8 µm powders has more patches of sintered area as compared to that from 0.8 µm powder. Only limited necking can be seen between the 0.8 µm particles in Figure 21. This is a clear indication that the part containing the 0.3 µm & 0.8 µm particles underwent better sintering than the part containing the 0.8 µm particles though the total loading of alumina in both parts was kept same, 60 vol. %.

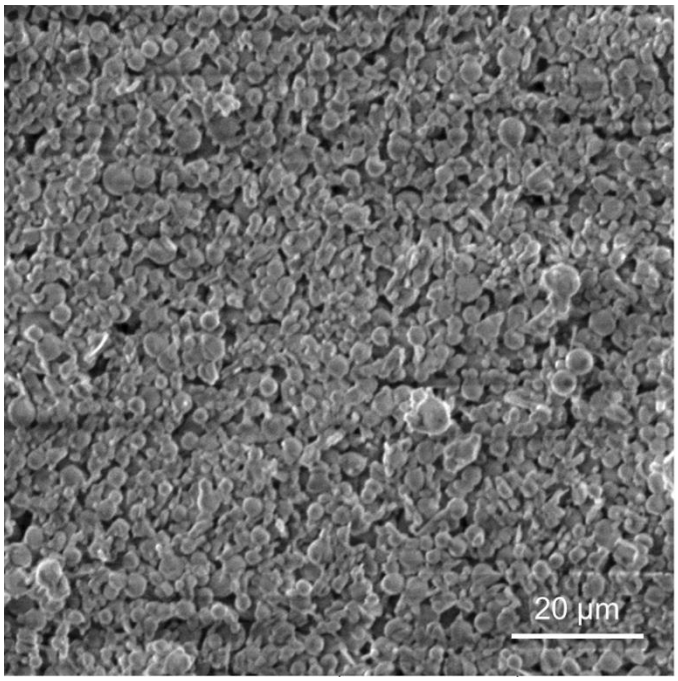

Figure 21: 0.8 µm particle printed and sintered part

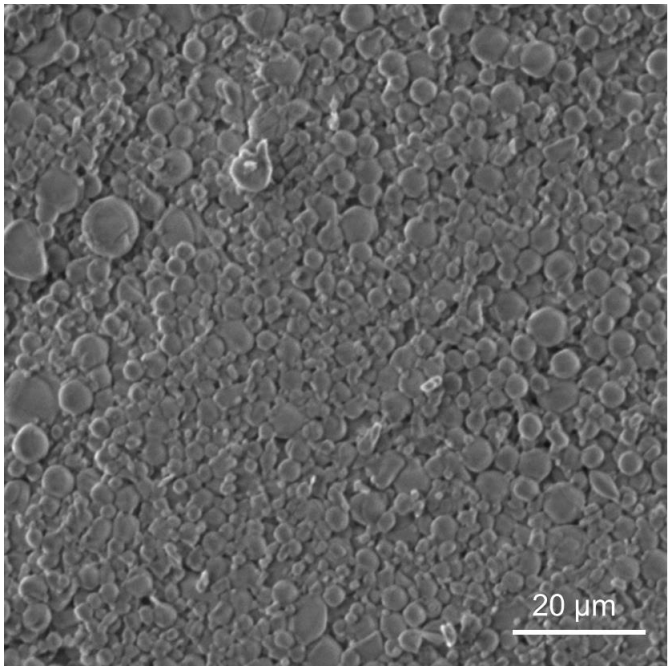

Figure 22: 0.3 µm & 0.8 µm particles printed and sintered part

5.4 SUMMARY

Alumina powder was mechanically mixed into an in-house photopolymerizable resin containing HDDA, dispersant (Oleic acid) and a photoinitiator (Diphenyl (2, 4, 6-trimethylbenzoyl) phosphine oxide). Using this suspension, ceramic green bodies of six different compositions were printed out using a vat photopolymerization printer. The effects of the alumina powders added as dopants on the sintered density and porosity were studied. The sample containing 0.3 µm particles achieved the highest density and the lowest porosity among the monomodal suspension. The sample containing 0.3 µm & 0.8 µm particles achieved the highest density and the lowest porosity among the bimodal suspension. This work demonstrated that ceramic structures can be produced by vat photopolymerization using a multimodal loading of ceramic particles in a photopolymerizable resin. Future work includes finding the optimal loading of the filler and dopant

material for the highest density of a ceramic part and also optimizing the amount of dispersant for a given composition of the alumina powder and the monomer.

CHAPTER VI

CONCLUSIONS

Two different indirect AM methods were investigated to produce feedstock for 3D printing of alumina. The first process investigated was the feasibility of the same using the indirect SLS method. A composite powder containing polyamide and alumina was prepared. The main conclusion drawn from the study was that the fraction of polyamide in the composite powder directly affected the flowability and sinterability of the powder. As the fraction of the polyamide in the composite powder increased, the flowability increased but the sinterability decreased. Hence, to produce high density ceramic parts a fine balance between the flowability and sinterability of the composite powder must be maintained.

For the second part of the study, the vat photopolymerization method was selected. A commercial photopolymerizable resin system was selected and ceramic 3D structures of different sizes using the same were printed. It was concluded that as the part size of the green bodies increased, for the same debinding and sintering profile, the sintered density and compressive strength of the sintered parts decreased.

From the vat photopolymerization using an in-house photopolymerizable resin in the third part of the study, a number of conclusions can be made some of which are: The size of the ceramic powder particles and the amount of loading in the suspension are the most important factor to produce 3D ceramic structures, the smaller the size of the powder particles, better the sinterability, the smaller the size for the powder particles chosen for the suspension, worse the flowability of the suspension.

It was also proven that size gradation of the powders helps in improving the final sintered density of the ceramic structures. Moreover, larger the gap in the particle size of the filler and dopant powder, higher the density change.

CHAPTER VII

FUTURE WORK

There is a strong motivation behind using vat photopolymerization for producing 3D structures with a myriad of applications in various industries. In the future, the current XYZprinting Nobel Superfine bottom up DLP printer can be modified to produce high density (> 95%) ceramic parts by supplementing it with a heating vat bed and a spreading mechanism for the suspension on the vat. These two appendages would enable the system to work with suspensions with much higher viscosities, thereby overcoming the current limitation.

The current resin ceramic system can be modified in a number of ways, some of which include changing the size and type of the ceramic powder and adding optimized amounts of dispersants for a given ceramic suspension system. Further studies can be conducted on the feasibility of producing dentures using yttrium stabilized zirconia using the same printer.

There is also scope of carrying out seminal work in terms of incorporating a feedback system into the printer which could automatically help decide the printing parameters of any type of filler material combined with a given system of the resin. That this addition would go a long way in democratizing the printing of functional parts using a wide variety of materials using a commercial DLP printer just with the click of a button.

REFERENCES

[Abdelrasoul 2015] Abdelrasoul, G.N., Farkas, B., Romano, I., Diaspro, A. and Beke, S., 2015. Nanocomposite scaffold fabrication by incorporating gold nanoparticles into biodegradable polymer matrix: Synthesis, characterization, and photothermal effect. Materials Science and Engineering: C, 56, pp.305-310.

[Agarwala 1996] Agarwala, M.K., Jamalabad, V.R., Langrana, N.A., Safari, A., Whalen, P.J. and Danforth, S.C., 1996. Structural quality of parts processed by fused deposition. Rapid Prototyping Journal, 2(4), pp.4-19.

[ASTM 2012] Standard, A.S.T.M., 2012. F2792. 2012. Standard Terminology for Additive Manufacturing Technologies. ASTM F2792-10e1.

[Bertsch 2003] Bertsch, A., Jiguet, S. and Renaud, P., 2003. Microfabrication of ceramic components by microstereolithography. Journal of micromechanics and microengineering, 14(2), p.197.

[Bogue 2016] Bogue, R. and Bogue, R., 2016. 3D printing: An emerging technology for sensor fabrication. Sensor Review, 36(4), pp.333-338.

[Chakravarthy 2010] Chakravarthy, K.M. and Bourell, D.L., 2010, August. Binder development for indirect SLS of non metallics. In Proceedings of the SFF Symposium pp. 81-90.

[Deckers 2012] Deckers, J., Kruth, J.P., Shahzad, K. and Vleugels, J., 2012. Density improvement of alumina parts produced through selective laser sintering of alumina-polyamide composite powder. CIRP Annals-Manufacturing Technology, 61(1), pp.211-214.

[Deckers 2016] Deckers, J.P., Shahzad, K., Cardon, L., Rombouts, M., Vleugels, J. and Kruth, J.P., 2016. Shaping ceramics through indirect selective laser sintering. Rapid Prototyping Journal, 22(3), pp.544-558.

[Du 2017] W. Du, X. Ren, C. Ma, and Z. Pei, 2017, “Binder Jetting Additive Manufacturing of Ceramics: A Literature Review,” Proceedings of the ASME 2017 International Mechanical Engineering Congress and Exposition, Tampa, FL, US.

[Edgar 2015] Edgar, J. and Tint, S., 2015. Additive manufacturing technologies: 3D printing, rapid prototyping, and direct digital manufacturing. Johnson Matthey Technology Review, 59(3), pp.193-198.

[Ebert 2009] Ebert, J., Özkol, E., Zeichner, A., Uibel, K., Weiss, Ö., Koops, U., Telle, R. and Fischer, H., 2009. Direct inkjet printing of dental prostheses made of zirconia. Journal of dental research, 88(7), pp.673-676.

[Farsari 2009] Farsari, M. and Chichkov, B.N., 2009. Materials processing: Two-photon fabrication. Nature photonics, 3(8), p.450.

[Formlabs 2017] https://formlabs.com/blog/3d-printing-technology-comparison-sla-dlp/

[Gallardo 2017] Gallardo, A., Pereyra, Y., Martínez-Campos, E., García, C., Acitores, D., Casado-Losada, I., Gómez-Fatou, M.A., Reinecke, H., Ellis, G., Acevedo, D. and Rodríguez-Hernández, J., 2017. Facile one-pot exfoliation and integration of 2D layered materials by dispersion in a photocurable polymer precursor. Nanoscale, 9(30), pp.10590-10595.

[German 1987] German, R.M., 1987. Theory of thermal debinding. Int. J. Powder Metall., 23(4), pp.237-245.

[German 2014] German, R., 2014. Sintering: from empirical observations to scientific principles. Butterworth-Heinemann.

[Gmeiner 2015] Gmeiner 2015 Additive Manufacturing of Bioactive Glasses and Silicate Bioceramics

[Goodridge 2007] Goodridge, R.D., Wood, D.J., Ohtsuki, C. and Dalgarno, K.W., 2007. Biological evaluation of an apatite–mullite glass-ceramic produced via selective laser sintering. Acta biomaterialia, 3(2), pp.221-231.

[Griffith 1996] Griffith, M.L. and Halloran, J.W., 1996. Freeform fabrication of ceramics via stereolithography. Journal of the American Ceramic Society, 79(10), pp.2601-2608.

[Grida 2003] Grida, I. and Evans, J.R., 2003. Extrusion freeforming of ceramics through fine nozzles. Journal of the European Ceramic Society, 23(5), pp.629-635.

[Guo 2013] Guo, N. and Leu, M.C., 2013. Additive manufacturing: technology, applications and research needs. Frontiers of Mechanical Engineering, 8(3), pp.215-243.

[Gu 2017] Gu, J., Liang, C., Zhao, X., Gan, B., Qiu, H., Guo, Y., Yang, X., Zhang, Q. and Wang, D.Y., 2017. Highly thermally conductive flame-retardant epoxy nanocomposites with reduced ignitability and excellent electrical conductivities. Composites Science and Technology, 139, pp.83-89.

[ISO 2003] ISO 18754, 2003. Fine Ceramics (Advanced Ceramics, Advanced Technical Ceramics) - Determination of Density and Apparent Porosity.

[Halloran 2011] Halloran, J.W., Tomeckova, V., Gentry, S., Das, S., Cilino, P., Yuan, D., Guo, R., Rudraraju, A., Shao, P., Wu, T. and Alabi, T.R., 2011. Photopolymerization of powder suspensions for shaping ceramics. Journal of the European Ceramic Society, 31(14), pp.2613-2619.

[Halloran 2016] Halloran, J.W., 2016. Ceramic stereolithography: additive manufacturing for ceramics by photopolymerization. Annual Review of Materials Research, 46, pp.19-40.

[Hatzenbichler 2012] Hatzenbichler, M., Geppert, M., Gruber, S., Ipp, E., Almedal, R. and Stampfl, J., 2012. DLP-based light engines for additive manufacturing of ceramic parts. In Proc. of SPIE, 8254, pp. 82540E-1.

[Hon 2008] Hon, K.K.B., Li, L. and Hutchings, I.M., 2008. Direct writing technology—Advances and developments. CIRP Annals, 57(2), pp.601-620.

[Jang 2000] Jang, J.H., Wang, S., Pilgrim, S.M. and Schulze, W.A., 2000. Preparation and characterization of barium titanate suspensions for stereolithography. Journal of the American Ceramic Society, 83(7), pp.1804-1806.

[Klocke 1997] Klocke, F., 1997. Modern approaches for the production of ceramic components. Journal of the European Ceramic Society, 17(2-3), pp.457-465.

[König 1991] König, W. and Verlemann, E., 1991. Machining Advanced Ceramics—A Challenge in Production Technology. In Designing with Structural Ceramics (pp. 187-200). Springer, Dordrecht.

[Kolan 2011] Kolan, K.C., Leu, M.C., Hilmas, G.E., Brown, R.F. and Velez, M., 2011. Fabrication of 13-93 bioactive glass scaffolds for bone tissue engineering using indirect selective laser sintering. Biofabrication, 3(2), p.025004.

[Liu 2012] Liu, K., Li, C.H., He, W.T., Shi, Y.S. and Liu, J., 2012. Investigation into indirect selective laser sintering alumina ceramic parts combined with cold isostatic pressing. In Applied Mechanics and Materials (Vol. 217, pp. 2217-2221). Trans Tech Publications.

[Nachum 2016] Nachum, S., Vogt, J. and Raether, F., 2016. Additive Manufacturing of Ceramics: Stereolithography versus Binder Jetting, Ceramic forum international: CFI. Berichte der Deutschen Keramischen Gesellschaft 93 No.3, pp.E27-E33.

[Özkol 2010] Özkol, E., Wätjen, A.M., Bermejo, R., Deluca, M., Ebert, J., Danzer, R. and Telle, R., 2010. Mechanical characterisation of miniaturised direct inkjet printed 3Y-TZP specimens for microelectronic applications. Journal of the European Ceramic Society, 30(15), pp.3145-3152.

[Pham 2006] Pham, T.A., Kim, D.P., Lim, T.W., Park, S.H., Yang, D.Y. and Lee, K.S., 2006. Three‐Dimensional SiCN Ceramic Microstructures via Nano‐Stereolithography of Inorganic Polymer Photoresists. Advanced Functional Materials, 16(9), pp.1235-1241.

[Prescott 2000] Prescott, J.K. and Barnum, R.A., 2000. On powder flowability. Pharmaceutical technology, 24(10), pp.60-85.

[Shahzad 2012] Shahzad, K., Deckers, J., Boury, S., Neirinck, B., Kruth, J.P. and Vleugels, J., 2012. Preparation and indirect selective laser sintering of alumina/PA microspheres. Ceramics International, 38(2), pp.1241-1247.

[Shahzad 2013] Shahzad, K., Deckers, J., Kruth, J.P. and Vleugels, J., 2013. Additive manufacturing of alumina parts by indirect selective laser sintering and post processing. Journal of Materials Processing Technology, 213(9), pp.1484-1494.

[Sirringhaus 2003] Sirringhaus, H. and Shimoda, T., 2003. Inkjet printing of functional materials. MRS bulletin, 28(11), pp.802-806.

[Subramanian 1995] Subramanian, K., Vail, N., Barlow, J. and Marcus, H., 1995. Selective laser sintering of alumina with polymer binders. Rapid Prototyping Journal, 1(2), pp.24-35.

[Sukeshini 2013] Sukeshini, M., Meisenkothen, F., Gardner, P. and Reitz, T.L., 2013. Aerosol Jet® Printing of functionally graded SOFC anode interlayer and microstructural investigation by low voltage scanning electron microscopy. Journal of Power Sources, 224, pp.295-303.

[Singh 2011] Singh, P., Smith, L.S., Bezdecny, M., Cheverton, M., Brewer, J.A. and Venkataramani, V., 2011, October. Additive manufacturing of PZT-5H piezoceramic for ultrasound transducers. In Ultrasonics Symposium (IUS), 2011 IEEE International (pp. 1111-1114). IEEE.

[Tang 2010] Tang, H.H., Tang Lee Huey-Ru, 2010. Method and apparatus for making three-dimensional parts. U.S. Patent Application 12/489,741.

[Trombetta 2017] Trombetta, R., Inzana, J.A., Schwarz, E.M., Kates, S.L. and Awad, H.A., 2017. 3D printing of calcium phosphate ceramics for bone tissue engineering and drug delivery. Annals of biomedical engineering, 45(1), pp.23-44.

[Utela, 2008] Utela, B., Storti, D., Anderson, R. and Ganter, M., 2008. A review of process development steps for new material systems in three-dimensional printing (3DP). Journal of Manufacturing Processes, 10(2), pp.96-104.

[Venkataraman 2000] Venkataraman, N., Rangarajan, S., Matthewson, M.J., Harper, B., Safari, A., Danforth, S.C., Wu, G., Langrana, N., Guceri, S. and Yardimci, A., 2000. Feedstock material property–process relationships in fused deposition of ceramics (FDC). Rapid Prototyping Journal, 6(4), pp.244-253.[Williams 2008] Williams, C.B., 2008. Design and development of a layer-based additive manufacturing process for the realization of metal parts of designed mesostructure. Georgia Institute of Technology.

[Wozniak 2011] Wozniak, M., de Hazan, Y., Graule, T. and Kata, D., 2011. Rheology of UV curable colloidal silica dispersions for rapid prototyping applications. Journal of the European Ceramic Society, 31(13), pp.2221-2229.

[Wu 2007] Wu, Y., Du, J., Choy, K.L. and Hench, L.L., 2007. Laser densification of alumina powder beds generated using aerosol assisted spray deposition. Journal of the European Ceramic Society, 27(16), pp.4727-4735.

[Xing 2015] Xing, J.F., Zheng, M.L. and Duan, X.M., 2015. Two-photon polymerization microfabrication of hydrogels: an advanced 3D printing technology for tissue engineering and drug delivery. Chemical Society Reviews, 44(15), pp.5031-5039.

[Yardimci 1996] Yardimci Atif, M. and Güçeri, S., 1996. Conceptual framework for the thermal process modelling of fused deposition. Rapid Prototyping Journal, 2(2), pp.26-31.

[Yeong 2013] Yeong, W.Y., Yap, C.Y., Mapar, M. and Chua, C.K., 2013, September. State-of-the-art review on selective laser melting of ceramics. In High Value Manufacturing: Advanced Research in Virtual and Rapid Prototyping. Proceedings of the 6th International Conference on Advanced Research in Virtual and Rapid Prototyping (p. 65). CRC Press.

[Zhou 2013] Zhou, C., Chen, Y., Yang, Z. and Khoshnevis, B., 2013. Digital material fabrication using mask-image-projection-based stereolithography. Rapid Prototyping Journal, 19(3), pp.153-165.

[Zocca 2015] Zocca, A., Colombo, P., Gomes, C.M. and Günster, J., 2015. Additive manufacturing of ceramics: issues, potentialities, and opportunities. Journal of the American Ceramic Society, 98(7), pp.1983-2001.